NASA TECHNICAL
MEMORANDUM

NASA TM X–62,091

NASA TM X–62,091

ESTIMATION OF MICROWAVE ABSORPTION IN THE JUPITER ATMOSPHERE

by William C. Coombs

Ames Research Center
Moffett Field, Calif., 94035

September 1971

FOREWORD

The basic study reviewed herein was formally reported by J. W. Davenport of RCA Laboratories under NASA contractor report CR-114288. This report adds to the original equations and formulations supplementary discussions of theory, laboratory verification of theoretical deductions, and application of empirical results to diverse model atmospheres.

This document was prepared as a combination of tutorial paper and application guide for communications engineers seeking to bridge gaps of understanding between the spectroscopy branch of physics and interplanetary spacecraft engineering practice. Because of vital implications of the physical theory in affecting the application of the study results to diverse model atmospheres, this paper provides previously unreported details of the absorption investigation and the intended area of application.

In the preparation of this document, acknowledgement is given to Dr. A. A. Maryott, for explanation and techniques of measurement during the course of laboratory verification measurements in the Gaithersburg, Maryland facility of the National Bureau of Standards. Additional information notes are also acknowledged from J. W. Davenport, the contract study's principal investigator, particularly as a consequence of his oral presentation of the subject at Ames Research Center, on September 2, 1971. Acknowledgement is given to R. L. Cramer of Ames Research Center who reviewed the manuscript, prepared the section

discussing the absorption coefficient and provided numerous mathematical insertions. In addition, he has supplied a glossary to facilitate understanding of terminology used in microwave spectroscopy.

The microwave-absorption task work reviewed herein was conducted under Phase II of Contract NAS2-5310 by RCA Laboratories. This task was initiated before the Jupiter-atmosphere models that Jet Propulsion Laboratory formulated in its atmospheric-entry studies program (Contract JPL 952811 with Martin Company and Contract JPL 952897 with Avco Corporation) became available. Accordingly, microwave-absorption studies reported under Phase II of the RCA contract were confined to the upper atmosphere of Jupiter as described by Moroz, Trafton, Wrixon, Michaux, Owen, Goodman, and others, based on astronomical and spectroscopic observations of the visible part of the upper atmosphere. The Phase-II work also was not intended to consider losses either due to scattering, dispersion, or other phenomena resulting from the particle-nature (for example, ice crystals) of the propagation medium or due to ionization, refraction, multipath, and other loss effects that are not of absorptive type. These effects will be reported under Phase-III program studies.

1. INTRODUCTION

Estimation of microwave absorption of the Jupiter atmosphere involves two different investigative study disciplines: (a) the determination of an acceptable model of the atmosphere itself, describing the composition, or constituency, as a function of temperature and partial pressures, as the abundance of each applicable element and compound varies with altitude through the total atmospheric profile; (b) the determination of the microwave attenuation rate applicable to each different volume sample of the atmosphere, and the integration of this loss over the varying radio-propagation path for any given entry trajectory, to obtain the total loss.

Principal reliance for definition of the atmospheric model rests with planetary scientists who base their deductions on observations by astronomers (including radio astronomers) and use infrared spectroscopy, as well as astrophysical and chemical analysis. Resolution of applicable microwave-loss rates depends heavily on the use of past planetary spectroscopic microwave-absorption-observation experience, studies of similar atmospheric constituents, and laboratory measurements simulating special model aspects believed to be unique to Jupiter.

This report is concerned primarily with the procedure for estimating the microwave-absorption loss once a model atmosphere has been defined in detail. However, experience with the evaluation procedure has shown such intricate dependence on subtle

features of atmospheric definition that it has been found desirable to include considerable model discussion in order to assure the proper application of the microwave-absorption formulations that have evolved from the study and experimental investigations. A glossary of terms commonly used in microwave spectroscopy is included to familiarize the reader with the terminology used in this report.

2. EVALUATION OF ABSORPTION CHARACTERISTICS -- GENERAL REMARKS

In the interest of expeditious evaluation of ammonia characteristics as they may pertain to microwave propagation in the Jupiter atmosphere, attention has been given to the vast amount of study and experimental measurements of ammonia already reported in the literature. We are reminded [42] that the ammonia molecule was the first to be studied by microwave-spectroscopy methods. It was the first molecule to reveal an inversion spectrum and a sharp microwave-line spectrum. It was the first to reveal power-saturation effects. It was the first to allow confirmation of the Van Vleck-Weisskopf theory of pressure-broadening at moderate pressures, as well as the first to show the inadequacy of this theory at much higher pressures. In addition to large amounts of practical data from early application to refrigeration, ammonia has been the subject of very precise theoretical investigations in connection with atomic clocks and masers.

It would be exceedingly costly to re-examine the many facets of ammonia characteristics already determined which would apply to some extent to the gamut of variations of temperature, partial pressures, and relative abundances of all the elements and compounds hypothesized to exist in the Jupiter atmosphere, and all the frequencies of transmission that might be considered for radio transmission through the atmosphere. For radio communications, using currently hypothesized atmospheric models, the range of variation

for Jupiter entry extends (at least) from 0.00001 atm to 1000 atm in pressure and from 100°K to 1500°K in temperature. The frequency range of interest extends from about 0.1 GHz to 10 GHz.

There would be formidable problems in attempting to measure directly in a laboratory the actual microwave absorptions for all combinations of temperature, pressure, partial pressures, abundances, and frequencies for hypothesized Jupiter models. To begin with, ammonia is so extraordinarily active that the very low partial pressure and ammonia abundances which are important in the Jupiter atmosphere would be lost almost immediately by absorption or by assimilation into the walls or surfaces of any metals (or nonmetals) that might be used in the pressure gauges, cavities, and connective tubing of the measurement system. At the high end of the pressure scale leakage becomes a problem at all joints and tuning bushings; and the very high temperatures that accompany high pressure (corresponding to the lower Jupiter atmosphere) cause melting of solder, brazing compounds, and other materials used to seal the system. Difficulties are experienced particularly at S-band and lower frequencies (of most interest to communications) because of the dimensional limitations for accommodating the electrical wavelengths in cavities and other tuning devices.

A practical approach to the absorption-measurement problem is to accept the techniques of combined observation, deduction, and empirical formulation that have been verified over a long period of study. To the extent that particular aspects of variation have been

verified by meticulous experiments and supporting theory, the work of others reported in such standard texts as Townes and Schawlow [9] or in journals has accordingly been used directly where a clear correlation of values is indicated. On the other hand, uncertainties in data due to changes of composition involving different proportions of hydrogen and helium in conjunction with ammonia have had to be checked in the laboratory at a sufficient number of temperatures and pressures to verify either conformity with or the need for amendment of established theory and empirical formulations.

Besides the classical Van Vleck-Weisskopf line-shape theory, as reported by Townes and Schawlow, important references used in the study-investigation include Ben-Reuven [10], concerning impact broadening of microwave spectra; Bleaney and Loubser [11], concerning the inversion spectra of ammonia at high pressures; Maryott, Birnbaum, Kryder, and Lyons [18], [20], [21], concerning absorption of various ammonia gases; Morris and Parsons [22], concerning ammonia absorption at very high pressures; and Ho, Kaufman, and Thaddeus [24], concerning absorption by water vapor.

The particular domain of ammonia pertinence to the Jupiter environment, which seems to have eluded specific prior investigation by researchers who have studied particular aspects of ammonia spectroscopic absorption, is that of various mixing ratios with hydrogen and helium at high pressures. Although significant, the

absorption by the hydrogen constituent itself is not substantial when compared to that of ammonia. However, the effect of hydrogen and, to a lesser extent, helium, in adding their partial pressures as foreign-body-line-broadeners of the ammonia spectra is extremely important. Methane and water vapor were tentatively expected to be important microwave absorbers in the Jupiter atmosphere, but examination of the abundances allowed by the most accepted current model atmospheres does not make them competitive, by orders of magnitude, with the levels of loss caused by ammonia.

The fact that measurement cavities for S-band and lower frequencies have very limited tuning ranges, which would necessitate constructing an indefinite number of relatively large separate tunable cells to cover the total VHF and UHF frequency bands of interest, is a major factor supporting the line-spectra-curve technique of measurement and empirical analysis. By this technique, establishment of absorption values at the extremely sensitive K-band frequency of the peak-line spectral amplitude and at least one (preferably two) frequencies in the S- and X-band range quite precisely determines the asymptotic curvature of the frequency-response function in the less sensitive wing of the spectral-response curve far below S-band. This determination must be made, however, for each different line spectrum that produces absorption components in the frequency range of interest.

In order to enable readers who are not familiar with spectroscopic absorption techniques to understand more readily the theory of analysis and measurement verification conducted under Ames' investigative project, the following sections may serve as an introduction to the absorption phenomenon.

3. THE ABSORPTION OF RADIO ENERGY BY AMMONIA AT MICROWAVE FREQUENCIES

Since the nature of loss due to ammonia absorption of microwave energy is somewhat different from most attenuation factors, an understanding of the principles involved will help one to grasp more readily the need for rather complex formulations and seemingly indirect procedures for evaluating what the uninitiated might have expected to be a simple handbook multiplying constant.

First, it should be understood that the actual ammonia spectral-line frequencies, which characterize atomic orbital wavelengths, are in the infrared band, far above the radio frequencies of concern to communications in the Jupiter environment. The general range of the frequency band of interest to communications in the Jupiter relay link is from 0.1 to 10 GHz. This range will be further narrowed by design-optimization considerations.

The ammonia spectral frequencies of eventual concern are not the molecular electronic, vibrational, or rotational state frequencies, but rather the inversion frequencies of ammonia, of which some 66 or more have been identified in Jupiter spectral observations using infrared spectroscopy techniques. But, again, the inversion-line frequencies do not themselves occur in the radio band of interest as defined above. The inversion frequencies are much lower than the orbital frequencies associated with the atoms of the ammonia molecule and are centered mainly in K-band, with one particularly strong line at 23.4 GHz. The identified resonant response-line spectra are fairly

stable and repeatably observable. While the resonant peaks are capable of shifting somewhat under loaded circuit conditions when propagation paths are simulated through gas cells in the laboratory, the resonant peaks of the 66 or more lines do not shift significantly under the influence of communication frequencies. Accordingly, the inversion line frequencies, available in many handbooks, similarly do not provide direct answers to the absorption constants needed at X-, S-, L-, or lower band frequencies.

Rather, the loss at lower frequencies is due to spectral line broadening of the ammonia inversion-line resonant-response characteristic, which can occur in the Jupiter atmosphere as a result of increased pressure, and foreign-body-impact collision of the ammonia molecule with the free hydrogen (H_2) and helium (He) and other possible elements of the atmosphere. As with most electrical phenomena, a number of theories have been advanced to explain spectroscopic line broadening. At least three such theories have met with considerable credence among physicists. One fairly tangible concept, familiar to communication engineers, treats the involved gas volume as though it constitutes a cell within a resonant circuit, with a quality factor Q. Under a condition of foreign-body-impact by hydrogen and helium atoms, the quality factor is lowered, and excitation susceptibility broadens to wider frequencies, without substantial shift of the peaks, just as is the case in resonant circuits.

A more detailed concept, which aids greatly in understanding what is involved in the resultant formulation and why S-band or other low-range response has to be evaluated indirectly from K-band response phenomena, may be described as follows.

Within the ammonia molecule (NH_3), the three hydrogen atoms are arranged as an equilateral triangle, constituting the base of a pyramid with the nitrogen atom at the apex as shown in figure 1. Under the excitation of a resonant inversion-line frequency, the nitrogen atom makes periodic traversals through the hydrogen-base plane to an apex position on the opposite side of the base. Energy is required to break through the potential barrier of the hydrogen plane. Accordingly, the periodic traversals of the nitrogen atom within the ammonia molecule, at the inversion frequency, absorb energy from the exciting source. When the frequency of the exciting radio wave is <u>off</u> the resonant-line value, there are nevertheless moments of periodic correspondence of phase at which the radio frequency is capable of exciting the nitrogen atom into <u>starts</u> of sympathetic oscillations. However, as the phase of the exciting wave drifts away from the inversion-line-frequency wave, agitation at that particular line frequency either stops or temporarily shifts to a more favorable mode of the 66 or more inversion line frequencies. The nitrogen atom makes its back-and-forth traversals only for those short spans of time when the inversion phase very nearly matches

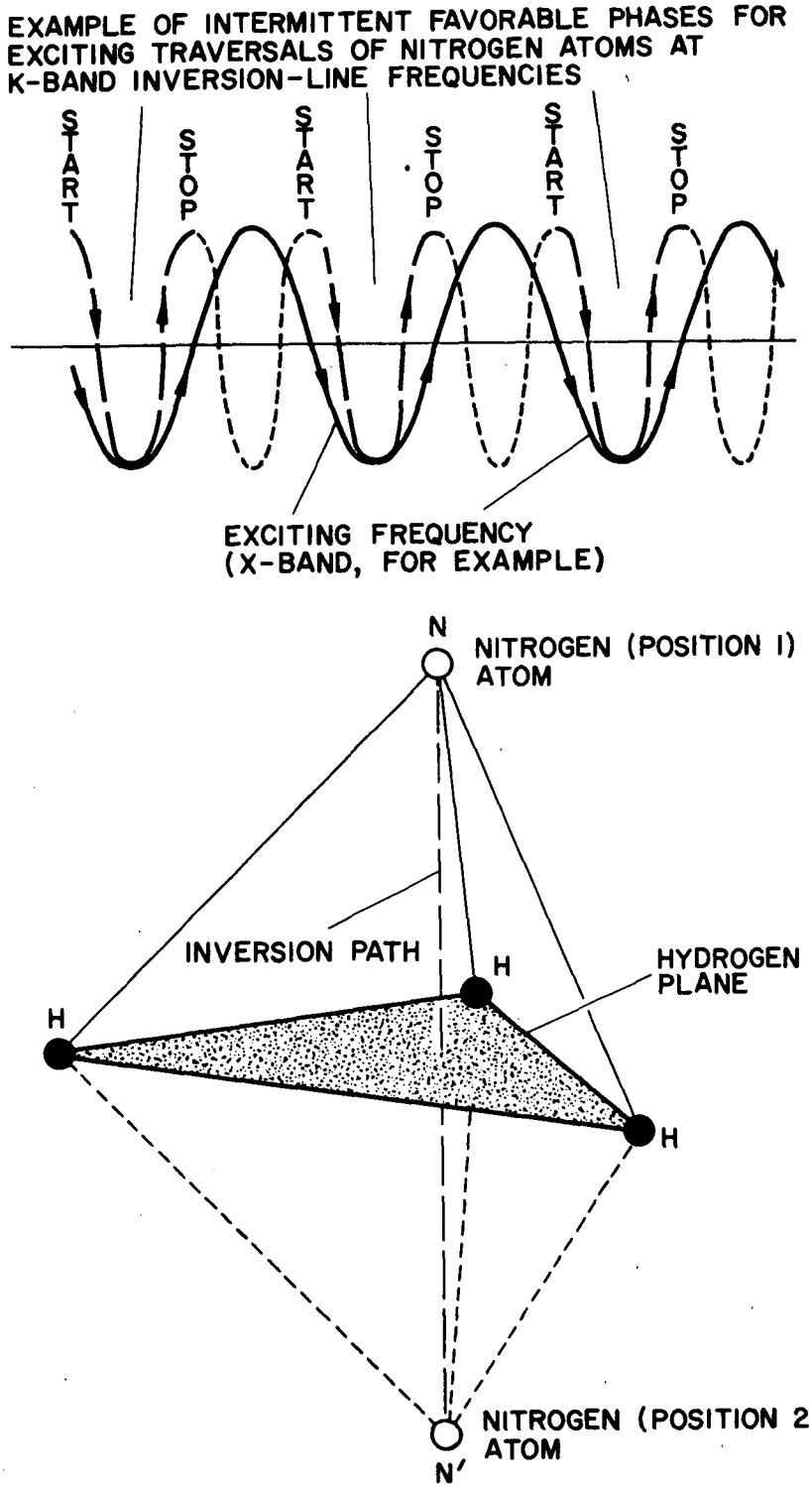

Fig. 1. Inversion of nitrogen atom within the NH_3-molecule.

the momentary excitation frequency phase. Once stopped, the vibratory processes start again almost immediately when the inversion atoms repeatedly sense semblances to the starting phases of their own inversion frequency. The remoteness of the exciting frequency determines the duration of sustained inversion oscillations and the degree to which energy will be absorbed before the exciting frequencies become so far out of phase with the inversion frequency that atomic inversion stops.

One consequence of increasing pressure, whether due to the partial pressure of ammonia or (to a lesser extent) the partial pressures of hydrogen and helium, is to increase the frequency of collision of ammonia molecules. The ammonia molecules emerge from collision essentially as before collision but with changes in phase due to the introduction of new frequency components during collision interaction. The change in phase due to each collision corresponds to a separate Fourier distribution of frequencies. Thus, the increase in the frequency of collision increases the likelihood and frequency of recurrence of the 66 or more phase states at which ammonia molecules become susceptible to inversion line stimulation by a microwave source of energy.

The net result of increasing pressure is that the total number of energy-absorbing inversions occurring in a given volume of ammoniated gas in unit time is increased. This trend of increasing absorption loss rate for any given communication frequency continues until a pressure is reached (somewhere in the vicinity of 15 to 20 atm, depending on the precise mixture of ammonia, hydrogen, and helium gases),

where pressure saturation effects begin to take place. Above this level, further addition of pressure tends to increase the molecular density to the point where the nitrogen atoms are further constrained from penetrating the hydrogen planes of the ammonia molecules. At the saturation peak absorption, this effect balances the effect of pressure in further increasing susceptible excitation phase states. Further additions of pressure will cause a decline in the absorption coefficient.

Thus, in modern terminology, the inversion line absorption mechanism may be likened to a kind of laser-pumping action or sympathetic pulsing or oscillation somewhat off the resonant frequency. The crucial point of understanding is that the energy absorption has to be fundamentally accounted for at the K-band inversion-line frequencies (by summing the effects). The response at lower exciting frequencies is determined as a loss of energy to support repeated false starts of oscillation by the nitrogen atom. This phasing of the oscillation starts is illustrated in the inserted sketch in figure 1.

This does not mean that, using sufficiently high ammonia abundances, one cannot go into a laboratory and measure directly the S-band absorption loss of ammonia. But the measurement could not be accurately extrapolated to any other frequency region without working through K-band to see what the governing consequences of the inversion-line frequency will be. For the low ammonia abundances of the Jupiter atmosphere, where the ammonia abundance is only about 2 torr at the top cloud level, such a direct measurement is, moreover, not practicable, since 2 torr of ammonia would be lost immediately in the walls of the

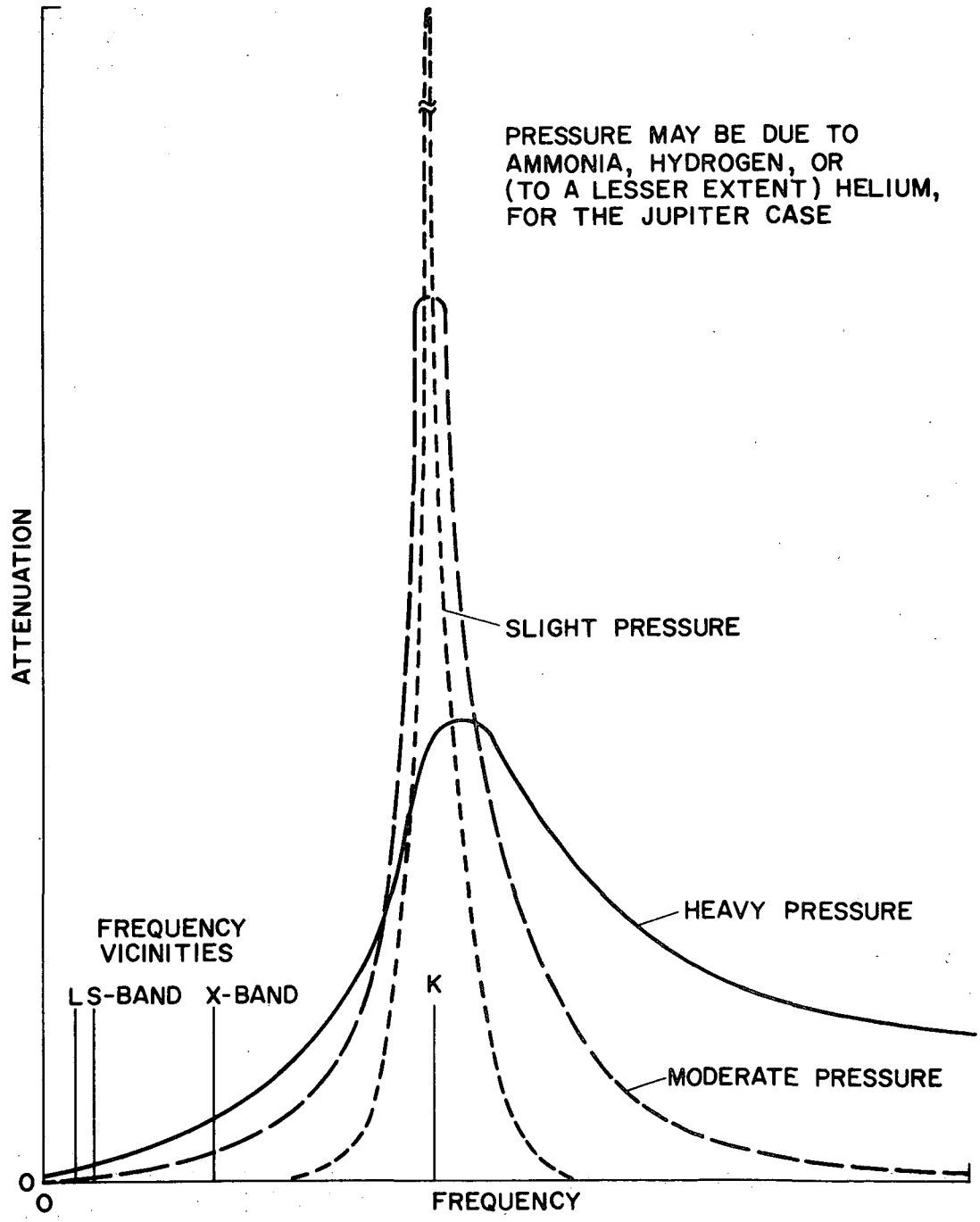

Fig. 2. Ammonia inversion-frequency spectral broadening.

measurement system. Instead, one must work with abundance values to which the available measurement system is sensitive. Fortunately, the required sensitivity for experimental study of the parameters applicable to Jupiter communication systems can be reached by translation through response envelope-shaping characteristics wherein ammonia abundance remains a linear parameter. This is the technique used in the subject investigation.

What one really establishes by theoretical analysis and laboratory verifications is the effect of each atmospheric parameter on the envelope-response extrapolation from K-band. Ammonia, hydrogen, and helium show different dependencies on temperature; and most of the parameters are involved in combinations when determining the absorption-curve shape. This results in a complex equation with coefficients that do not remain fixed over the total range of interest. This variability is not different from the Van Vleck-Weisskopf or the other classical formulations in which, for example, for certain line-broadening cases an inverse dependence on temperature is used, while for other cases an inverse square-root-temperature correspondence provides better experimental agreement.

In order to illustrate further the complexity of extrapolating (and graphically explaining what one is really doing in the process), reference is made to figure 2. Here, the central dotted graph near K-band represents the 23.4 GHz inversion line of ammonia under a slight pressure condition. The somewhat broader dashed graph represents the same line under a condition of moderate pressure, and the heavy

line shows the change of the absorption-response curve under strong pressure. Actually, in accordance with a spectroscopy theorem (of a conservation-of-energy nature), the total area under the varying curve remains almost constant. (In the graph, which is not to scale, the central resonance spike has been compressed disproportionately so that the lower structures may be compared more readily.)

The graphs illustrate the subtlety of the rise in attenuation at the lower frequencies, corresponding to the falling of the characteristic at K-band. Thus, note the complex situation: whereas certain factors, such as ammonia saturation, correspond to elevation of the characteristic throughout (from all lower frequencies up to the inversion-line frequency at K-band), other factors such as hydrogen and helium pressure elevate the L-, S-, and X-band absorptions of energy at the same time that they either do not change or actually depress K-band response. This implies complex transitions of values among the parameters, temperature, pressure, etc. Whereas in ordinary gas laws one thinks of temperature as increasing molecular activity, temperature has an inverse effect on the absorption in the S-band absorption vicinity or pressure-broadened spectra. The line broadening effects of ammonia, hydrogen, and helium not only have different individual dependencies on temperature but also have varying dependencies when extrapolations are made to greatly differing temperatures and pressures. Moreover, many of the control parameters cannot be simply accounted for individually in governing the absorption-characteristic curve but are best accounted for as responses coupled

with other parameters. This is a phenomenological explanation of the reason for the complex equations and formulations needed for evaluating ammonia absorption. Understanding along these lines makes it clear that these equations should not be removed from their analytical context and applied as formulae outside the bounds of their developmental constraints.

4. THE AMMONIA-ABSORPTION COEFFICIENT

The absorption spectrum of ammonia at microwave frequencies arises from a molecular transition called inversion, discussed in Section 3. The spectrum itself is described experimentally and theoretically by the so-called absorption coefficient, α, which is a function of the frequency ν of the electromagnetic wave illuminating a chemical sample (such as ammonia) in the gaseous state.

The inversion transition causes some 66 spectral lines between 17 and 40 GHz in the absorption spectrum. The value of the absorption coefficient $\alpha(\nu)$, at any frequency ν, is the sum of the contributions from the individual lines. Ordinarily, the absorption effect is significant only for frequencies near resonance -- this is, where α is maximum. However, the spectral lines may be broadened considerably by collisions between molecules in the gas sample as a consequence of increased pressure. Thus, the absorption effect of the 66 spectral lines extends to frequencies much lower than 17 GHz. In Earth's atmosphere, for instance, the spectral line of oxygen near 60 GHz is pressure-broadened and the absorption effect is noticeable throughout the microwave region starting at 1 GHz. The absorption effect exhibited by pure ammonia due to pressure-broadening of the spectral lines is shown in figure 3. This figure shows the left wing of the graph of the absorption coefficient α versus frequency ν when the ammonia-gas pressure is increased from 0.13 atm to 2 atm. It is clear from the figure that, at ν=1 GHZ, there is essentially no absorption when the pressure is 0.13 atm, while the absorption is nearly 20 dB/km when the pressure is 2 atm.

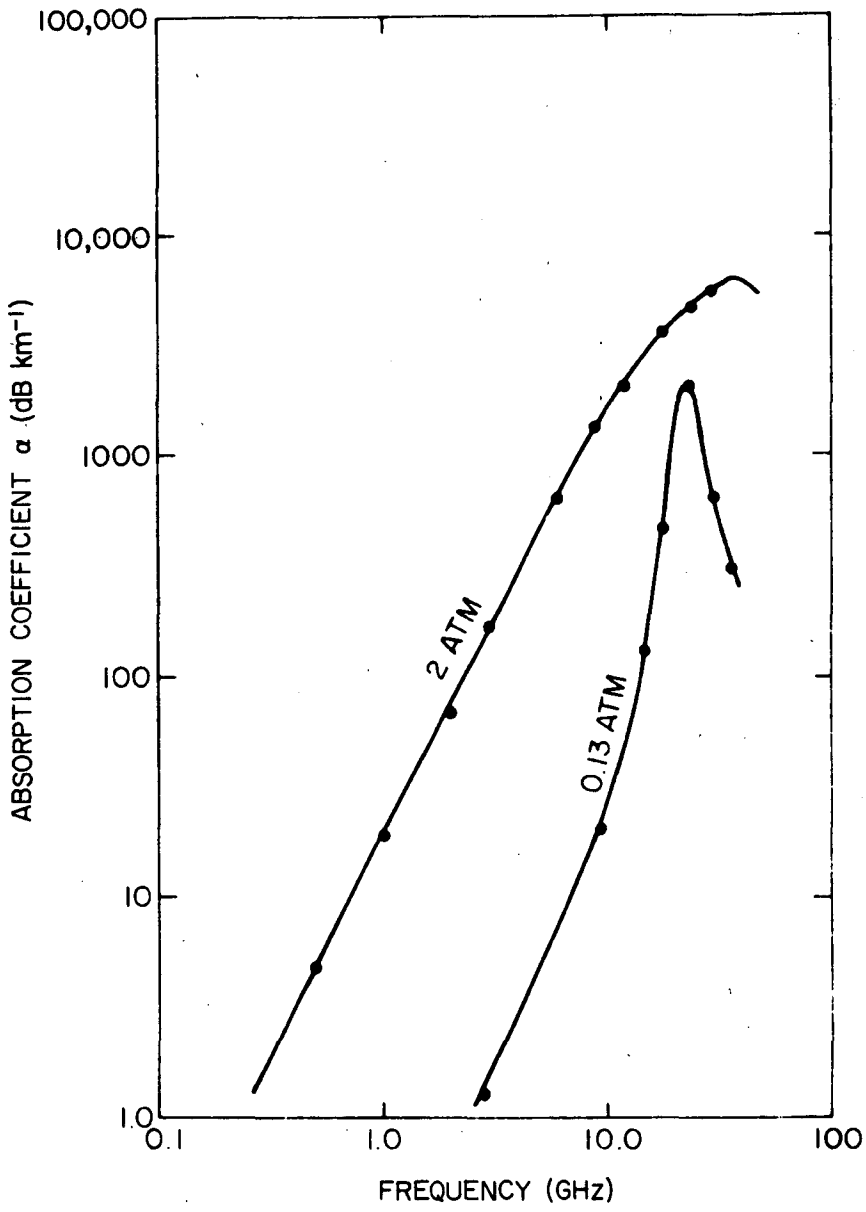

Fig. 3. Absorption coefficient α versus frequency ν for pure ammonia at two different pressures (11).

4.1 The Lorentz Expression

The derivation of the mathematical form of the absorption coefficient has been outlined by Townes and Schawlow [9]. The Lorentz relation for the absorption coefficient α_{ij} for a single spectral line near resonance is

$$\alpha_{ij}(\nu) = \frac{\pi f_i |\mu_{ij}|^2}{3ckT\,\epsilon_o} N \nu^2 \left[\frac{\gamma_{ij}}{(\nu - \nu_{ij})^2 + \gamma_{ij}^2}\right] \tag{4-1}$$

The symbols in this relation are:

f_i = fraction of the total number of absorbing molecules per unit volume in the lower state i of the two molecular states

$|\mu_{ij}|^2$ = square of the dipole-moment-matrix element μ_{ij} for a transition from the lower state i to the upper state j due to pressure (coulomb·meters)^2

c = speed of light = 3×10^8 m/sec

k = Boltzmann's constant = 1.38×10^{-23} joules/°K

T = temperature of the chemical sample whose absorption spectrum is to be obtained (°K)

ε_o = permittivity of free space = 8.85×10^{-12} farad/m

N = total number of absorbing molecules per unit volume (m^{-3})

ν = excitation frequency (Hz)

ν_{ij} = resonance frequency for transition from state i to j (Hz)

γ_{ij} = frequency of molecular collisions in the gas (Hz)

$= \frac{1}{2\pi\tau}$

τ = mean time between molecular collisions in the gas (sec).

The collision frequency γ_{ij} is the product of the number N_s of scattering molecules per unit volume (which may be different from the number N of absorbing molecules), the thermal velocity v, and the collision cross section σ_{ij}, that is,

$$\gamma_{ij} = N_s \, v \, \sigma_{ij}$$

The function in brackets of Eq. (4-1) has a maximum at the frequency $\nu=\nu_{ij}$, and the half-width at half-maximum is γ_{ij} (in Hz). Figure 4 illustrates this. It is simply a shifted Cauchy density, known from probability theory [41]. The graphical appearance of the product ν^2 times the bracketed function, which is $\alpha(\nu)$ up to a scale factor, is shown in figure 5. This figure makes it clear that $\alpha(\nu)$ rises as ν^2 for frequencies less than the maximum that occurs at $\nu=(\nu_{ij}^2 + \gamma_{ij}^2)/\nu_{ij}$. For large frequencies, the curve approaches 1 asymptotically. Thus, the area under the curve, interpretable as the mean-square value of a Cauchy density, is infinite.

Apart from the graphical appearance, a number of physical observations can be made about α of Eq. (4-1). Since the absorption coefficient increases approximately as ν^2 for frequencies below resonance, the absorption (in dB/km) increases by a factor of roughly 20 from S- to X-band. α is proportional to the number of absorbing molecules per unit volume

$$N = \frac{P}{kT}$$

where P is the partial pressure of the absorbing molecules. For example, near the cloud layer of Jupiter, the partial pressure of ammonia rises exponentially as the altitude of maximum ammonia density is approached (see Section 7). Therefore, a large increase in absorption is to be expected there. Finally, provided that the total pressure is below approximately 10 atm, the absorption coefficient increases linearly with the collision frequency γ_{ij}, which, in turn, is proportional to the

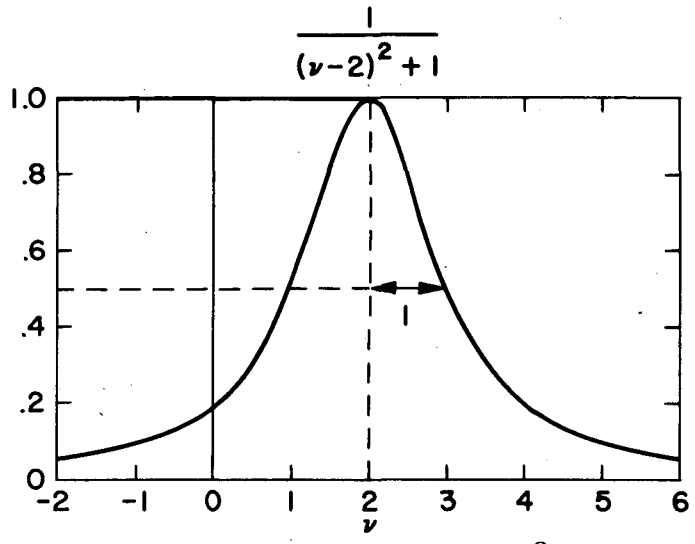

Fig. 4. The Lorentz shape-factor $1/\left[(\nu-2)^2+1\right]$ in Eq. (4-1).

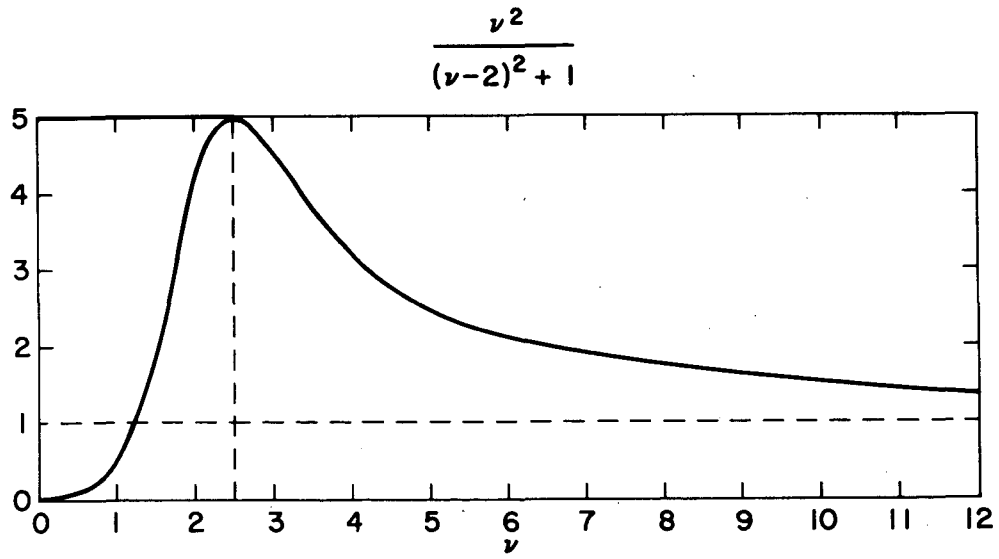

Fig. 5. The term $\nu^2/\left[(\nu-2)^2+1\right]$, for ν positive, in Eq. (4-1).

partial pressure of the scattering gas (via the number N_s of scattering molecules per unit volume). To take account of a mixture of gases, consisting of ammonia (NH_3), hydrogen (H_2), and helium (He), we sum the effect of each constituent to obtain the collision frequency†

$$\begin{aligned}\gamma &= \gamma_{NH_3} + \gamma_{H_2} + \gamma_{He} \\ &= (a\,P)_{NH_3} + (a\,P)_{H_2} + (a\,P)_{He}\end{aligned} \tag{4-2}$$

The γ's are the collision frequencies of the chemical substances, as subscripted, which would be observed for each substance acting individually. The P's are partial pressures (in newton/m^2). The a's are coefficients allowing us to write the formula

$$\gamma = aP$$

from the proportionality $\gamma \propto P$; the a's are determined experimentally (see Section 8). The increase in γ with pressure is the reason for the term "pressure broadening" of a spectral line in the absorption spectrum.

---

† The subscripts ij are omitted for clarity since we will be considering dominant values for the overall absorption curve.

It was remarked previously that 66 lines have been observed in the ammonia-inversion spectrum. Therefore, the sum

$$\alpha = \sum_{ij} \alpha_{ij}$$

is tedious to calculate. The computation can be simplified by replacing the quantities ν_{ij} and γ_{ij} with their dominant values ν_o and γ, respectively, and summing the dipole-moment-matrix elements

$$\sum_{ij} f_i \left|\mu_{ij}\right|^2,$$

weighted by the proportion f_i of the absorbing molecules in the lower state i. Then the overall absorption coefficient due to the inversion-frequency spectral lines becomes

$$\alpha(\nu) = \frac{\pi}{3c\,k\,T\,\epsilon_o} \left[\sum_{ij} f_i \left|\mu_{ij}\right|^2\right] N \nu^2 \frac{\gamma}{(\nu - \nu_o)^2 + \gamma^2} \tag{4-3}$$

where ν_o is the dominant inversion-line frequency, γ the dominant collision frequency, and ν is the communication frequency. For ammonia, ν_o = 23.4 GHz. The term

$$\frac{\gamma}{(\nu - \nu_o)^2 + \gamma^2} \tag{4-4}$$

is called the Lorentz shape factor.

The sum in brackets has been computed [33] for the most intense lines; the result is

$$\sum_{ij} f_i \left|\mu_{ij}\right|^2 \cong 0.40\,\mu^2 = 9.6 \times 10^{-60}\ (\text{coulomb} \cdot \text{m})^2$$

where $\mu = 4.90 \times 10^{-30}$ coulomb·m is the dipole moment of the non-vibrating molecule. Thus, for calculations, Eq. (4-3) can be written

$$\alpha(\nu) = 2.7453 \times 10^{-34} \frac{N}{T} \nu^2 \frac{\gamma}{(\nu - \nu_o)^2 + \gamma^2} .$$

4.2 The Van Vleck-Weisskopf Expression

A second form for the absorption coefficient α has been formulated by Van Vleck-Weisskopf [9] from a modification of Lorentz's assumption concerning the state of the molecule after a collision. When the pressure is high, or above about 1 atm, the experimental curve for α is well described by the Van Vleck-Weisskopf expression. When the pressure is well below 1 atm, this expression is good only near the spectral line-resonance frequency ν_o, not for microwave excitation frequencies that are far below ν_o. When dominant values are substituted, their expression is

$$\alpha(\nu) = \frac{2\pi}{3c\,k\,T\,\epsilon_o}\left[\sum_{ij} f_i \left|\mu_{ij}\right|^2\right] N \nu^2 \left(\frac{\gamma}{(\nu - \nu_o)^2 + \gamma^2} + \frac{\gamma}{(\nu + \nu_o)^2 + \gamma^2}\right) \qquad (4\text{-}5)$$

The term in parentheses is called the Van Vleck-Weisskopf shape factor

$$\frac{\gamma}{(\nu - \nu_o)^2 + \gamma^2} + \frac{\gamma}{(\nu + \nu_o)^2 + \gamma^2} = \frac{2\gamma\,(\nu^2 + \nu_o^2 + \gamma^2)}{(\nu^2 - \nu_o^2)^2 + 2\gamma^2\,(\nu^2 + \nu_o^2) + \gamma^4}, \qquad (4\text{-}6)$$

which we have rewritten here for later use. The meaning of the symbols appearing here is the same as in the preceding section.

The first term of the Van Vleck-Weisskopf shape factor (4-6) is recognized as the Lorentz shape factor shown in figure 4. The second term of (4-6), taken by itself, is also of Lorentz shape but shifted to the negative frequency axis. Thus the overall appearance of (4-6) is the sum of two Cauchy densities that are symmetrical with respect to the vertical axis. The product ν^2 times the factor in parentheses

in Eq. (4-5) is shown in figure 6 for positive frequencies only. At low pressures, the collision frequency γ is small compared to the resonance frequency ν_o, so that the Van Vleck-Weisskopf shape factor approaches the Lorentz shape factor; that is, the first term in (4-6) predominates.

Eq. (4-5) has been used by a number of researchers (for example, [16] and [24]) to analyze the water-vapor absorption. This will be treated for the Jupiter atmosphere in Section 7.

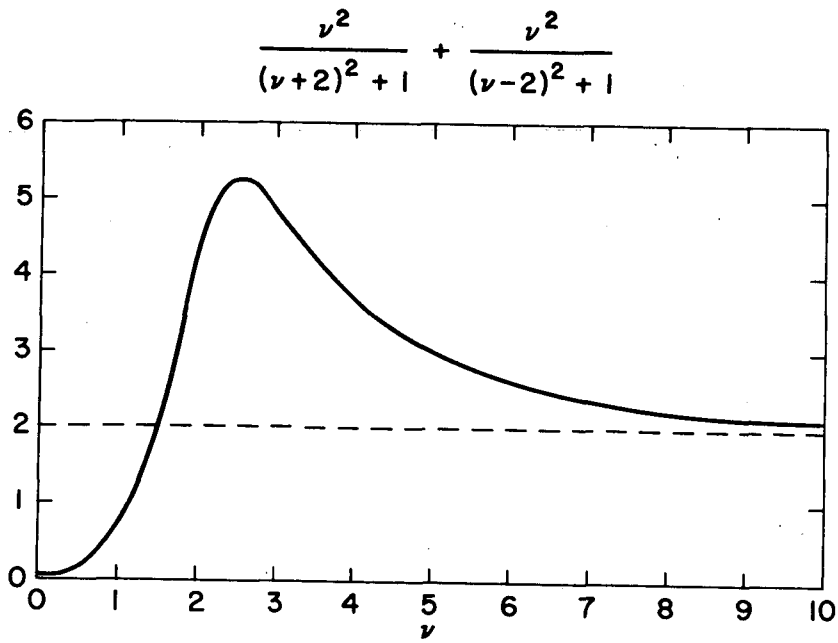

Fig. 6. The term $\nu^2/\left[(\nu+2)^2+1\right] + \nu^2/\left[(\nu-2)^2+1\right]$, for ν positive, in Eq. (4-5).

4.3 The Ben-Reuven Relation

A third form for the absorption coefficient α has been formulated by Ben-Reuven [10]. His investigation includes the assumption that a change in the molecular state may be caused by collisions themselves, whereas the preceding two theories assumed that state changes are caused only by incident radiation. Ben-Reuven's relation agrees well with experimental results over a large range of pressures and frequencies, especially pressures of a few atmospheres and those frequencies far from the spectral-line resonance frequency. The relation is

$$\alpha_{ij}(\nu) = \frac{\pi}{3c\,k\,T\,\epsilon_0} N \nu^2 \sum_{ij} \left[f_i \left| \mu_{ij} \right|^2 \mathcal{F}_i \right] \tag{4-7}$$

with

$$\mathcal{F}_i = \frac{2(\gamma_i - \zeta_i)\nu^2 + 2(\gamma_i + \zeta_i)\left[(\nu_{ij} + \delta_i)^2 + \gamma_i^2 - \zeta_i^2\right]}{\left[(\nu_{ij} + \delta_i)^2 + \gamma_i^2 - \zeta_i^2 - \nu^2\right]^2 + 4\gamma_i^2\nu^2} \tag{4-8}$$

If we again choose dominant values, Ben-Reuven's absorption coefficient α takes the form

$$\alpha(\nu) = \frac{\pi}{3ckT\epsilon_o} \left[\sum_{ij} f_i \left| \mu_{ij} \right|^2 \right] N \nu^2 \mathcal{F}(\nu) \tag{4-9}$$

with the Ben-Reuven shape factor

$$\mathcal{F}(\nu) = \frac{2(\gamma - \zeta)\nu^2 + 2(\gamma + \zeta)\left[(\nu_o + \delta)^2 + \gamma^2 - \zeta^2\right]}{\left[\nu^2 - (\nu_o + \delta)^2 - \gamma^2 - \zeta^2\right]^2 + 4\nu^2\gamma^2} . \tag{4-10}$$

The shape factor $\mathcal{F}$ depends on the applied microwave signal frequency ν and also on the collision frequency γ, the so-called coupling element ζ (a frequency which, like γ, is proportional to the number of scattering molecules per unit volume), the spectral line resonance frequency ν_o, and the shift parameter δ in the resonance frequency (which may be neglected for pressures below 100 atm). The dependency of these spectroscopic variables on the partial pressures of ammonia, hydrogen, and helium, and also on temperature, is indicated by

$$\mathcal{F}(\nu;\ \gamma,\ \zeta,\ \nu_o) = \mathcal{F}(\nu;\ P_{NH_3},\ P_{H_2},\ P_{He},\ T) .$$

The curve shaping factor must be evaluated for each set of applicable absorption parameters that prevail in the model atmosphere.

Eqs. (4-9) and (4-10) are the spectroscopic base on which this report is structured. However, the Ben-Reuven line shape does not apply to water vapor absorption; the Van Vleck-Weisskopf theory is used for that. Figure 7 shows the graphical appearance of Ben-Reuven's shape factor for the simple choices $\nu_o=2$, $\delta=0$, $\gamma=1$, and $\zeta=0.75$. The shape is clearly asymmetrical in comparison with the Lorentz shape factor. Figure 8 shows ν^2 times Ben-Reuven's factor which is the frequency-dependent term in the absorption coefficient α of Eq. (4-9). Note that $\mathcal{F}$ tends to 0 as ν tends to ∞.

The symbols appearing in Eqs. (4-9) and (4-10) are repeated for convenience:

f_i = fraction of the total number of absorbing molecules per unit volume in the lower state i of the two molecular states

$|\mu_{ij}|^2$ = square of the dipole-moment-matrix element μ_{ij} for a transition from the lower state i to the upper state j due to pressure $(\text{coulomb}\cdot\text{m})^2$

c = speed of light = $3\text{x}10^8$ m/sec

k = Boltzmann's constant = $1.38\text{x}10^{-23}$ joules/°K

T = temperature of the chemical sample whose absorption spectrum is to be obtained (°K)

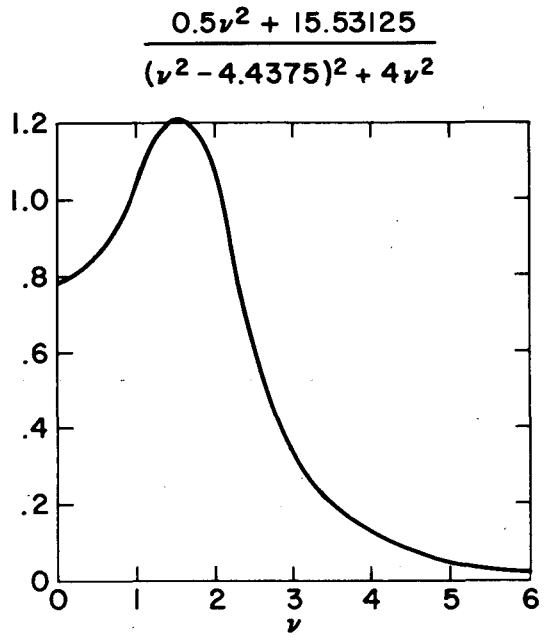

Fig. 7. Ben-Reuven's shape factor $\mathcal{H}(\nu)$ in Eq. (4-9). for $\nu_o = 2$, $\delta = 0$, $\gamma = 1$, $\zeta = 0.75$.

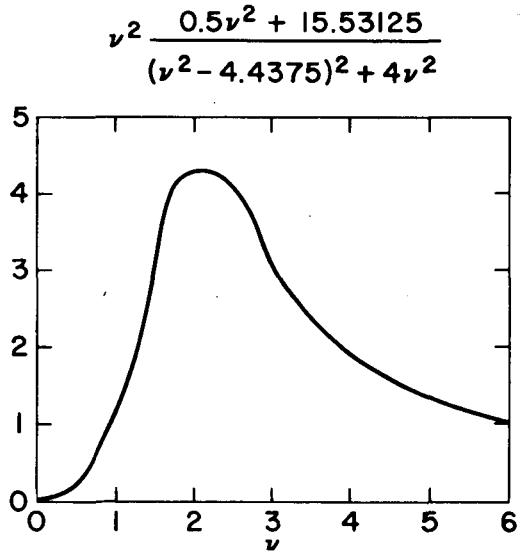

Fig. 8. The term $\nu^2\, \mathcal{F}(\nu)$ in Eq. (4-9) where $\mathcal{F}(\nu)$ is Ben-Reuven's shape factor with $\nu_o = 2$, $\delta = 0$, $\gamma = 1$, $\zeta = 0.75$.

ε_o = permittivity of free space = 8.85×10^{-12} farad/m

N = total number of absorbing molecules per unit volume (m^{-3})

ν = excitation frequency (Hz)

ν_o = dominant resonance frequency (Hz)

γ = frequency of molecular collisions in the gas (Hz)
= aP (a is given in Table 1)

ζ = coupling element (Hz)
= bP (b is given in Table 1)

P = partial pressure of the absorbing molecules (newton/m^2)

δ = shift in the resonance frequency due to pressures above 100 atm (Hz)

The new† feature of Ben-Reuven's shape factor (4-10) is the coupling element ζ which is not present in the Van Vleck-Weisskopf shape factor (4-6). The coupling element ζ arises from the mathematical description of the absorption process; physically speaking,

---

† It is assumed throughout that the shift parameter δ is negligible. This has been verified by experiment to be the case over the frequency range of interest. This parameter is, therefore, not shown in the Van Vleck-Weisskopf expression (4-5). When this assumption does not hold, that is, when the pressure is low, then ν_o must be replaced by $\nu_o + \delta$.

ζ represents collision-induced molecular transitions and relates to the width of the spectral line and to the resonance frequency under pressure-broadening. When $\zeta = 0$, the Ben-Reuven shape factor takes the form of the Van Vleck-Weisskopf shape factor.

The Ben-Reuven shape factor (4-10) may be approximated by simpler expressions depending on the application. The shift parameter δ is taken to be 0 throughout. When the pressure is low (less than 10 atm, say), then the pressure-dependent frequencies γ and ζ are much lower than the resonance frequency ν_o. In that case.

$$\mathcal{F}(\nu) \cong \frac{2(\gamma - \zeta)\nu^2 + 2(\gamma + \zeta)\nu_o^2}{(\nu^2 + \nu_o^2)^2} . \qquad (4\text{-}11)$$

If, in addition, the frequency ν of the applied microwave signal is much less than ν_o, then $\mathcal{F}$ reduces to a constant (with respect to ν):

$$\mathcal{F} \cong \frac{2(\gamma + \zeta)}{\nu_o^2} . \qquad (4\text{-}12)$$

This approximation leads to

$$\alpha(\nu) = \text{constant} \times \nu^2$$

for the absorption coefficient as a function of signal frequency. The study investigation has shown that this approximation is valid for frequencies less than 10 GHz.

For calculations, the following substitutions can be made in Eqs. (4-9) and (4-10):

$$N = \frac{P_{NH_3}}{kT}, \qquad P_{NH_3} = \text{partial pressure of ammonia}$$

$$\sum_{ij} f_i \left|\mu_{ij}\right|^2 \cong 0.4\,\mu^2 = 9.6 \times 10^{-60}\ (\text{coulomb} \cdot \text{m})^2$$

where $\mu = 4.90 \times 10^{-30}$ coulomb•m is the dipole moment of the non-vibrating molecule. Thus

$$\frac{\pi}{3ck^2\epsilon_o} \sum_{ij} f_i \left|\mu_{ij}\right|^2$$

$$= \frac{3.14 \times (9.6 \times 10^{-60}\ \text{coulomb}^2 \cdot \text{m}^2)}{3 \times (3 \times 10^8\ \text{m/sec}) \times (1.38 \times 10^{-23}\ \text{joules/°K})^2 \times (8.85 \times 10^{-12}\ \text{farad/m})}$$

$$= 1.9880 \times 10^{-11}\ \frac{\text{coulomb}^2 \cdot \text{m}^2 \cdot \text{sec} \cdot {}^\circ\text{K}^2}{\text{joules}^2 \cdot \text{farad}}\ .$$

The following further substitutions for physical units are made:

$$\text{capacitance} = \frac{\text{charge}}{\text{potential}}$$

$$1 \text{ volt} = \frac{1 \text{ joule}}{1 \text{ coulomb}} ;$$

$$\text{thus} \qquad \text{farads} = \frac{\text{coulomb}^2}{\text{joule}} ;$$

Furthermore,

$$1 \text{ joule} = 1 \text{ newton} \cdot \text{m}$$

so that

$$\frac{\pi}{3c\,k^2\,\epsilon_o} \sum_{ij} f_i \left|\mu_{ij}\right|^2 = 1.9880 \times 10^{-11} \frac{\text{m} \cdot \text{sec} \cdot {}^\circ\text{K}^2}{\text{newton}} . \tag{4-13}$$

The absorption coefficient of Eq. (4-9) can then be written

$$\alpha(\nu) = \left(1.9880 \times 10^{-11} \frac{\text{m} \cdot \text{sec} \cdot {}^\circ\text{K}^2}{\text{newton}}\right) \frac{P}{T^2} \nu^2 \mathcal{F}(\nu) \text{ m}^{-1} \tag{4-14}$$

where P (in newton/m^2) is the partial pressure of the absorber, T (in °K) is the temperature of the absorber, ν (in Hz) is the applied microwave signal frequency, and

$$\mathcal{F}(\nu) = \frac{2(\gamma - \zeta)\nu^2 + 2(\gamma + \zeta)(\nu_o^2 + \gamma^2 - \zeta^2)}{(\nu^2 - \nu_o^2 - \gamma^2 + \zeta^2)^2 + 4\nu^2\gamma^2} \quad \text{Hz}^{-1} \tag{4-15}$$

is Ben-Reuven's shape factor. The frequencies

$$\gamma = aP \quad \text{and} \quad \zeta = bP$$

are computed from the a and b coefficients that are determined experimentally (see Section 8). ν_o is the spectral-line resonance frequency of the absorber.

Examination of the Ben-Reuven theory shows that Eqs. (4-9) and (4-10) may be applied to the Jupiter-model atmospheres proposed by Neil Divine of the Jet Propulsion Laboratory. The model atmospheres of JPL are specified in tabular form showing the total pressure P, the partial pressures of the atmospheric constituents, the corresponding temperatures, and the height with reference to the P=1 atmosphere point. The remaining unknowns, γ and ζ, must be computed for each point considered. Since the procedure is tedious, the calculations should be mechanized.

5. UPPER-ATMOSPHERE MODELS DESCRIBED IN THE LITERATURE

An excellent analysis of the various model atmospheres has been given by Goodman [3]. Other sources on models are Michaux, Moroz, and Trafton [4], [5], [6]. Owen provides a discussion of the constituents of the atmosphere [7].

Description of the upper atmosphere of Jupiter (down to the lower vicinity of the top cloud level) is typified by the so-called Moroz "working model." This model is described in "Physics of Planets," a NASA-published translation (TT F-515, document N68-21802) of V. I. Moroz's work, which reviews the observations of leading planetary scientists. Moroz weighs the observations and conclusions of others and rationalizes plausible conclusions, based mainly on astronomic and spectroscopic data. Moroz's model conceptions are limited to the upper atmosphere, primarily because that is the only region in which positive infrared and optical data has been obtained.

For absorption-computation purposes, the following is a description of the Jupiter atmosphere based on a model by Moroz [5]. Jupiter is surrounded by a cloud layer thought to be several thousand km above the surface [8]. Above the clouds is a relatively clear atmosphere consisting almost entirely of hydrogen and helium. The temperature at the upper surface of the clouds is approximately 170°K, and the pressure is of the order of 2 atm (1 atm = 760 torr = 760 mm of Hg). The constituents and their amounts† are H_2 = 85 ± 15 km-atm, He = 10 to 100 km-atm, CH_4 = 0.050 km-atm, and NH_3 = 0.007 km-atm.

---

† 1 km-atm = 2.69×10^{28} m^{-2}. It is a measure of the number of molecules in the atmosphere per unit surface area of the planet. For convenience, this is converted into the length of the column which would be obtained if the gas were compressed to STP (at a temperature of 273°K). For 1 km-atm, this length is 1 km.

These are values given by Owen [7]. The uncertainty in the helium concentraction is taken into account in the following calculations. Clearly, the atmospheric processes are dominated by H_2 and He. However, the absorption at both microwave and infrared frequencies is basically due to NH_3 and CH_4.

In the stratosphere (assuming T = constant) of Jupiter, the pressure and density follow an exponential law:

$$P(z) = P(0) \exp(-z/h) \tag{5-1}$$

where $h = \frac{kT}{mg}$ = scale height†, P(0) is a reference pressure and z is the altitude above a reference. Here, $k = 1.38 \times 10^{-23}$ Joules $(°K)^{-1}$ is Boltzmann's constant, m is the mean molecular mass of the layer, and $g = 26 m(sec)^{-2}$ is the acceleration due to gravity on Jupiter. For H_2, h ≈ 28 km. For NH_3, h is much less because m is greater. However, because of the saturation effects discussed below, the ammonia distribution is not governed by Eq. (5-1). Jupiter is assumed to have an atmosphere above the cloud layer in which the temperature varies linearly with height z above the cloud layer (in the Moroz model):

$$T(z) = T(0) - \gamma_a z \tag{5-2}$$

---

† The scale height measures the relationship between density and temperature at any point in an atmosphere. It may be regarded as the thickness of a homogeneous atmosphere (having a density constant with height) which would give the observed temperature. For a planetary atmosphere, scale height is often determined by occultation observations or by observations of the disappearance of a star behind the planet.

$\gamma_a = g/c_p$ = adiabatic temperature gradient

c_p = specific heat at constant pressure

$T(0)$ = temperature at reference point (170°K in the Moroz model).

This troposphere would be expected to be from 20 to 30 km thick. Since c_p is about 10^4 joules $(kg\ °K)^{-1}$, γ_a is about $2.5°K\ (km)^{-1}$. In the troposphere the pressure is related to the temperature by the adiabatic law

$$P(z) = P(0)\left[T(z)/T(0)\right]^{\gamma/(\gamma - 1)} \qquad (5\text{-}3)$$

where γ is the ratio of specific heats at constant pressure and volume ($\gamma = 1.4$ for H_2).

There is evidence [7] that the ammonia vapor is saturated near the cloud tops. This means that its partial pressure is just the vapor pressure which can be obtained from the Clausium-Clapeyron equation. The partial pressure of ammonia is

$$P_{NH_3} = P_o \exp\left[-23\left(\frac{T_o}{T} - 1\right)\right] . \qquad (5\text{-}4)$$

The subscript "o" refers to cloud-top values. P_o is about 2.4 torr if T_o is taken to be 170°K [15]. The number of molecules per unit volume, N, is given by $N = P(kT)^{-1}$.

Goodman [3] has discussed the various absorbers at microwave frequencies and has shown that ammonia is by far the strongest. To be sure, water vapor absorbs at these frequencies; but even if there were equal amounts of water and ammonia, the absorption due to H_2O would be only about 2 percent that due to NH_3 (see Section 7). Hydrogen also has a collision-induced absorption spectrum, but it is not important below about 10 GHz.

6. OTHER APPLICABLE MODEL ATMOSPHERES

The basic microwave-ammonia-absorption studies under Ames' investigative program have been undertaken with a view toward application to any of the outer planetary atmospheres where ammonia, hydrogen, and helium are dominant constituents. The basic determinations, including measurement data, are quite general but expected to require changes of scaling factors when applied over very broad ranges. Scaling factors for applying absorption equations have been verified only for the upper atmosphere of Jupiter, in the RCA Phase-II studies. Application to pressures greater than about 7 atm in the Jupiter atmosphere will involve the introduction of pressure saturation and other factors which are being formulated under Phase-III studies.

The only substantial models which have been advanced to represent the unseen lower atmosphere of Jupiter are the so-called Lewis (M.I.T) and JPL models. These models attempt to link lower-atmosphere plausibilities with upper-atmosphere observations, to present overall consistency of upper and lower atmospheres. Constituency of the lower atmosphere is deduced largely from computational estimates of gravity effects on known atmospheric elements and compounds of the solar system that could conceivably exist on Jupiter, in accordance with their known molecular masses. Using further assumptions of atmospheric stability (implying convective equilibrium), Lewis and JPL have rationalized how the atmosphere might be layered down to about 1,000 atm pressure.

In order to cover certain atmospheric exigencies, they have hypothesized at least three quite different models of temperature-pressure relationship. For purposes of communication-system design, the JPL model atmospheres have been rather precisely defined at 5 km intervals over an altitude span of about 200 km, corresponding to pressures from 0.2 atm to 530 atm, for the cool, dense model. This preciseness of definition should not be confused with relative validity considerations when compared with the simplistic but observation-supported models suggested by Trafton, Moroz and others, for the upper atmosphere region. The validity of all of the models is highly contingent on the dynamic stability of the atmosphere, a factor which is not yet definitely known in the case of Jupiter.

Unfortunately, there has been no standardization among astronomers as to exactly what temperature and pressure or altitude should correspond to the "top" of the ammonia cloud layers. Indeed, this would be difficult to specify because the clouds are arranged not in discrete shells but in varying altitudes in belts or zones around Jupiter. There are also holes and plateaus in the cloud levels. Just as clouds clear at times on Earth, so also do they on Jupiter, to a limited extent. The different temperatures and pressures assigned by astronomers to the top of the cloud level do not necessarily indicate basic disagreement so much as the fact that nobody has ever claimed to have located the cloud level in relation to a precise altitude, within at least ten or more kilometers. Lacking standardization, observers have assigned their own scales of reference, corresponding to some zero altitude.

Until recently, the differences did not appear to be of great consequence in the astronomical sense, since the atmosphere is believed to extend many hundreds of kilometers below the cloud top, with commensurate increases of temperature to many hundreds of degrees Kelvin below the cloud layers. However, with respect to microwave absorption due to ammonia in the Jupiter atmosphere, the zero-altitude reference choice becomes very important. In comparing the Moroz and JPL models, it is not only the apparent difference in parameter values in the very broad vicinity of the ammonia cloud layer that matters but, more importantly, the inplication of different model concepts. To a considerable extent, the choice of models is a matter of judging what one can realistically accept while maintaining consistency with the total history of observations. When only the upper atmosphere (above the cloud layer) is at issue, Moroz's model probably agrees most with past astronomical data. On the other hand, by postulating a somewhat different upper-atmosphere model, JPL and Lewis are able to add more credence to a quite tenable theoretical lower-atmosphere model, while reconciling comparatively recent additions of theory regarding the upper atmosphere of Jupiter.

In accordance with his use of an altitude where T = 170°K as a convenient zero-altitude reference commensurate with an assumption of convective equilibrium and an adiabatic gradient within the region of formation of the observable ammonia bands, Moroz sets an upper limit of 175°K on the temperature and a lower limit of 150°K. Many

Jupiter-observation scientists, including Kuiper, Squires, and Trafton, assign top cloud-temperature-reference values within this range.

Using revisions of their own earlier models, JPL/Lewis, for a "cool, dense" model of Jupiter, assume a zero-altitude reference at a point where the total pressure is 1 atm, which corresponds, in their model, to a temperature of only 144°K. But on the other hand, their zero-reference temperature is 180°K for a "nominal" atmosphere and 238°K for a "warm, extended" model atmosphere. While the uninitiated might construe the spread of these figures as representing "cover-the-field" estimates on Lewis' or JPL's part, these temperature assumptions are actually the result of careful consideration.

In order to have a convenient reference coarsely in the vicinity of the cloud level, JPL somewhat arbitrarily adopted a zero-altitude reference corresponding to 1 atm, which is the region in which we see clouds on Earth. But this "reference" has no express definition in relation to the top of the ammonia-cloud layer as such and does not provide a common reference point for correlating the "cool, dense," "nominal," and "warm, expanded" JPL models with the Moroz and other models. Rather, the point at which the JPL models are based in definition and should be compared in concept to other models (after a proper temperature-pressure-correspondence determination) is 125°K. The pressure correspondence at this level is 0.3 atm for the "nominal" JPL model. The correspondence with the other JPL models is simply that a so-called "cool, dense" model is defined as having a pressure correspondence of +0.2 atm higher, and a so-called "warm, expanded" model is defined as having a pressure 0.1 atm lower

than the nominal 0.3 atm at 125°K.

The 125°K-temperature has no special ammonia-cloud-layer significance in the JPL models. Rather, 125°K is chosen as a stable relative opacity or transmissibility reference for spectroscopic observations into the cloud region or to top of the lower atmosphere. At the 12-micron wavelength used for this reference, the dominant atmospheric absorber is hydrogen (H_2), not ammonia. It is pertinent that the same temperature of 144°K that is assigned to the 1-atm-pressure level in the "cool" model, corresponding to 180°K in the "nominal" model, will be reached again in the upward direction above the stratosphere. At the same supra-stratosphere level, the "warm" model reaches 500°K. The latter figure is the result of observational opinion by James Warwick of the University of Colorado Observatory who believes that temperatures in the Jupiter upper atmosphere may change this much due to changes in the solar cycle. This does not proportionately affect ammonia-absorption determinations at the cloud level, but a difference of only -0.1 or +0.2 atm of pressure at the 125°K-temperature-pressure-correspondence point can imply widely differing temperatures among the three JPL models at any given level, either up or down from the reference level. In relation to ammonia abundance, these temperatures imply interpretations of observations in the JPL models different from those of the so-called Moroz model. In order to understand these differences, further background information is necessary.

As explained by Moroz, two different model concepts of the Jupiter atmosphere have received prominent attention. These concepts represent efforts to explain the total visual and infrared data that have been spectroscopically observed. One is a direct reflectance concept that uses direct reflection from the cloud layers as a basis for accounting for observed data. The other is a multiple-scattering model. All observers seem to agree that ammonia must condense within the temperature range of 130-200°K and that ammonia gas may exist in a state of saturation in equilibrium with liquid and solid (frozen) states over much of this temperature range. Under this condition, Moroz considers it unrealistic to interpret the apparent observed atmospheric abundance levels of ammonia, methane, and hydrogen as direct-reflectance values. He believes that the observed spectral-line broadening must be in part due to multiple scattering.

Moroz found that his multiple-scattering model allowed consistent correlation with observed differences in ammonia abundance, above and below his mean-value determination, in the different belts and zones around Jupiter. On the other hand, he found no basis for correlating observed differences in spectral intensity of the ammonia bands to either temperature, pressure, or particulate (frozen) matter differences, using a direct-reflectance model. Moroz should not be regarded as overly-conservative in over-allowing for ammonia abundance. Although he agrees with the range of temperature values

observed by Kuiper, Squires, and others, Moroz assigns less than half the ammonia partial pressure or abundance that Kuiper and others have, in the multiple-scattering model.

However, adherents of the direct-reflectance theory conceived an additional hypothesis, to overcome observational objections to their direct-reflectance theory. This hypothesis is that a supracloud layer exists above the prominent ammonia-cloud region, which compensates for the spectroscopic discrepancies when the direct-reflectance theory is applied to cloud-region observations. Moroz does not accept this hypothesis because he considers it unrealistic to believe that compensation could be in the precise amount needed, even if the effect exists. He considers the scattering coefficient allowed by the compensation hypothesis to be too low, by an order of magnitude. It is significant that Moroz himself determined that the Jupiter "working model" commonly associated with his name (total pressure equal to about 3.8 atmospheres in the cloud vicinity) would have to be reduced by a factor of three in regard to gaseous abundance and partial pressures of hydrogen, helium, ammonia, and methane, if one were to accept the supracloud-compensation hypothesis.

On the other hand, JPL's model concept is stated in terms of transmissibility or relative opacity, which is more appropriate for comparing observable data with the computational models of the lower Jupiter atmosphere. The JPL "nominal" model reference of pressure-temperature correlation (0.3 atm at 125°K) allows the

presumption of an adiabatic troposphere (the same as Moroz's) but implies an essentially isothermal stratosphere, and requires an inversion layer to reconcile rising temperatures above the stratosphere (consistent with Warwick's evaluations), at the same time that temperatures rise with decreasing altitude below the stratosphere.

The same magnitude of temperature that Moroz would assign in the cloud vicinity as 170°K at 3.8 atm pressure corresponds to 2.3 atm in JPL's "cool" model, 0.85 atm in JPL's "nominal" model, and 0.5 atm in JPL's "warm, extended" model. Corresponding to an ammonia partial pressure of 2.5×10^{-3} atm for the Moroz model at 170°K, the JPL models' ammonia partial pressures are 6.0×10^{-4} atm for the "cool" model, 1.4×10^{-4} atm for the "nominal" model, and 3.9×10^{-5} atm for the "warm, extended" model. As previously noted, the JPL temperature reference is taken at 125°K, a temperature below that at which ammonia condenses.

Thus, Moroz's upper atmosphere description and Lewis/JPL's lower atmosphere description do not meet in a common altitude reference. Accordingly, they cannot be compared directly with respect to ammonia absorption at particular altitudes within the region of most critical interest -- from the top to the bottom of the ammonia cloud -- except as one may justify singling out either temperature, pressure, or other parameter, as a basis for common reference, notwithstanding differences in all remaining parameters. This lack of a common

altitude reference has some important implications in handling the absorption equations deduced by RCA for application to the upper atmosphere as defined by Moroz, when direct comparisons are attempted with the lower atmosphere as defined by Lewis or JPL.

Use of the Phase-II report's analytic-deduction equations beyond the depth of the upper cloud layer to at least a few atmospheres is permissible provided the temperature difference does not change greatly from the range studied. The range of satisfactory application of equations, insofar as temperature is concerned, extends over the range of JPL models, or from about 100°K to at least 500°. Since the JPL "cool, dense" model starts with a lower temperature than the Moroz model in the troposphere, somewhere above the cloud layer, and gets hotter with increasing depth or pressure, a point will ostensibly be found at which temperature figures corresponding to Moroz's cloud level are reached. But the temperature correspondence to pressure and ammonia abundance is different because of the difference in model concepts and reference points, so that careful attention to model details is required. As previously noted, Moroz himself would require a reduction in the apparent observed ammonia abundances and partial pressures by a factor of three, if one chooses to believe the supracloud-compensation hypothesis. On the other hand, in the JPL models, the temperatures can have widely different altitude correspondences for only very minor differences in pressure at the JPL reference point.

RCA's absorption formulation in the Phase II report remains consistent with stated development and application constraints. But RCA's Phase-II contract requirement for the evaluation of direct-entry and occultation trajectories in the upper atmosphere must not be lifted out of the context of upper-atmosphere ranges of parametric variation and be applied to JPL's differently defined models unless there is careful correlation of all reference assumptions and constraints over the interval of comparison. This requires careful study; consideration of changes of formulation coefficients which may be required for the greater extremes of pressure that apply to the lower atmosphere is a major task of the Phase-III study. However, the computation procedure itself remains the same.

Pending availability of the Phase III results, in making absorption-loss comparisons between different model atmospheres, the details of model definition must be examined further than what relates to the absorption-rate (per km) parameters. For example, due to the fact that Moroz's "working model" prescribes a higher ammonia abundance in the cloud vicinity than some other models, Moroz's model has been somewhat arbitrarily decried as pessimistic, from a radio-propagation-loss standpoint. Actually, when one examines the relative scale heights over which the ammonia loss must be integrated in the different models to get the total path loss, certain of the lower-rate models may be found to yield a greater total loss than Moroz's "working model." Similarly, if one chooses to believe in the supracloud-compensation hypothesis and applies Moroz's factor-of-three reduction to the abundance

and partial-pressure figures of his "working model," Moroz's model will become optimistic compared with other models.

These considerations suggest that, in the general application of data results, confusion will be avoided if model atmospheres are designated in accordance with their detailed qualitative and quantitative descriptions instead of the authors' names. It is apparent that scientists will advance new thoughts from time to time, and their various published reservations and qualification cannot be counted on to be assembled in a single reference, nor are they necessarily representative of their most recent thinking.

In this connection, it should be noted that the parametric values used by RCA in computations for curves appearing in the Phase-II report are as stated in the report. The RCA model includes modifications of the model by Trafton and others, as noted. RCA does not particularly espouse one model over another; and, as previously noted, the Phase-III work (which is being done jointly by RCA and Ames in-house investigations) is using models defined by Neil Divine of JPL and John S. Lewis of M.I.T.

7. ABSORPTION DUE TO WATER VAPOR

It has been mentioned that the water-vapor absorption is expected to be much less than the ammonia absorption, at least above the cloud layer. A rough indication of this is contained in figure 9, where the H_2O absorption coefficient for Earth is shown. However, a more detailed comparison will now be made.

First, to our knowledge, water vapor has not been detected in Jupiter's atmosphere [7] but has been predicted on the basis of thermodynamic calculations by Lewis [23]. Therefore, the distribution of H_2O with height is uncertain. We will assume that the water vapor is saturated at each temperature; this is a worst-case analysis since, in any event, no more water vapor could exist in equilibrium.

The microwave-absorption spectrum for water vapor consists solely of transitions among the various rotational energy levels of the molecule. There is no "ammonia-like" inversion transition. The line shape for each transition can be computed from the Van Vleck-Weisskopf expression (see equation (4-5)).

$$\alpha(\nu) = \frac{2\pi}{3c\,k\,T\,\epsilon_o} N \nu^2 \sum_{ij} f_i \left|\mu_{ij}\right|^2 \left[\frac{\gamma_i}{(\nu - \nu_{ij})^2 + \gamma_i^2} + \frac{\gamma_i}{(\nu + \nu_{ij})^2 + \gamma_i^2}\right]. \qquad (7\text{-}1)$$

Notice that there is an additional factor of 2 in Eq. (7-1) compared with Eq. (4-7). This is due to the inversion transition in NH_3, which doubles the number of states and therefore halves the number

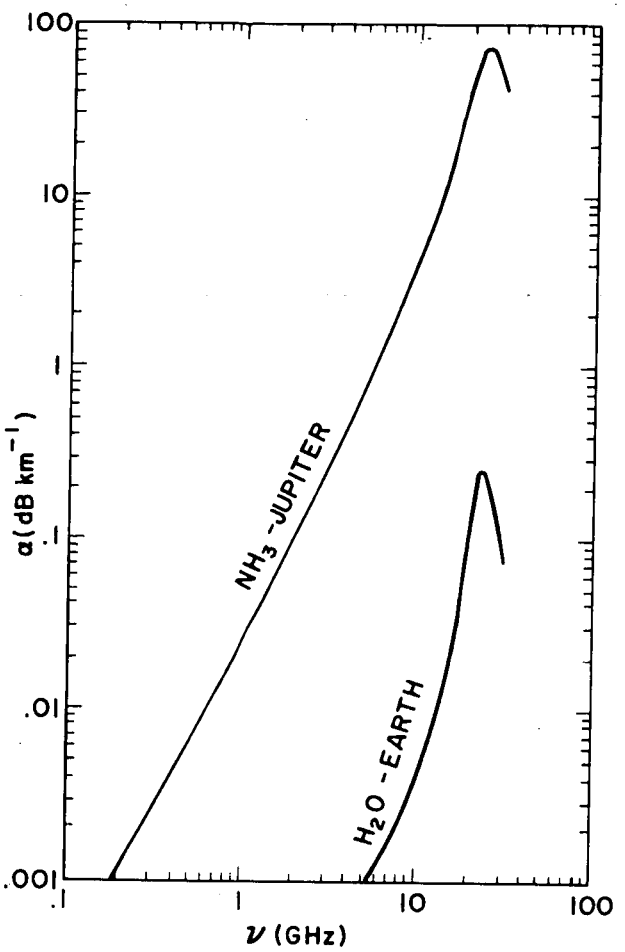

Fig. 9. Absorption coefficient α versus frequency ν at the Jovian cloud top. P_{H_2} = 2 atm, P_{He} = 1.4 atm, P_{NH_3} = 2 torr, T = 170°K. For comparison, the absorption due to a mixture of water vapor in air for a typical earth day is shown. The water vapor partial pressure is about 9 torr.

of absorbing transitions for the ammonia case. Eq. (7-1) has been used by many authors [16], [24] to analyze water-vapor absorption; the Ben-Reuven line shape (Eq. 4-7) does not apply to water vapor.

The lowest transition has a frequency of 22.2 GHz and is the most important for low pressures (less than 1 atm). At higher pressures, the higher lines become so broad that they dominate. Ho, Kaufman, and Thadeus [24] have studied the water-vapor spectrum when broadened by N_2 at sufficiently high pressures that the 22.2 GHz line may be neglected. They have summarized their results in a formula which in our notation is

$$\alpha = 6.2 \times 10^{-3} \frac{P_{H_2O} P \nu^2}{(\text{atm})^2 (\text{GHz})^2} \left(\frac{273}{T}\right)^{3.1} \text{dB} \cdot \text{km}^{-1} \qquad (7\text{-}2)$$

where T is the absolute temperature, P_{H_2O} is the partial pressure of water vapor, and P is the total pressure. It might appear that α decreases with increasing T, but actually P_{H_2O} rises exponentially with T if we assume the water vapor to be saturated. Eq. (7-2) is consistent with Eq. (7-1) because $\nu_{ij} \gg \nu$ and $\nu_{ij} \gg \gamma_{ij}$. We also recall that $\gamma_{ij} \propto P/T$ and $N \propto P_{H_2O}/T$. The additional factor $T^{0.1}$ comes from a slight additional temperature dependence of γ with T. This formula represents only part of the H_2O-absorption at pressures of a few atmospheres or less. Assuming T = 273°K and P = 2 atm with the water-vapor saturated ($P_{H_2O} = 6 \times 10^{-3}$ atm), we obtain (for ν = 2.315 GHz)

$$\alpha \cong 4 \times 10^{-4} \text{ dB} \cdot \text{km}^{-1} .$$

To this must be added the absorption due to the 22.2 GHz line. This has been treated for Earth by Van Vleck [16]. He also uses Eq. (7-1) but with ν_{ij} = 22.2 GHz and γ = 3 GHz. Again, assuming a temperature at the cloud tops of 273°K (a very high value; clearly a worst case) and a total pressure of 2 atm, we find

$$\alpha_{22.2\ \mathrm{GHz}} = 1.3 \times 10^{-4}\ \mathrm{dB} \cdot \mathrm{km}^{-1}.$$

Therefore, the absorption in this case due to H_2O is $\alpha = 5.3 \times 10^{-4}$ dB/km. This is less than 1 percent of the NH_3 absorption. Furthermore, the water-vapor concentration is almost certainly much less than that assumed (273°K). Therefore, above the clouds, water-vapor absorption may be neglected.

Finally, note that all H_2O-data are for nitrogen, rather than hydrogen, as the foreign gas. This should overestimate the absorption on Jupiter by a small factor [9] but in any event should be accurate to within 25 percent.

8. EXPERIMENTAL EVALUATIONS

8.1 Laboratory Technique

As previously indicated, the goal of the Ames measurements program was to determine the actual corrections of parametric variation which should be substituted in classical spectral-line-broadening formulae, preparatory to determining the absorption values that would apply over the range of pressures, temperatures, and relative abundances of ammonia, hydrogen, and helium, in currently theorized Jupiter models. Many different techniques of measurement have been described in the literature with varying degrees of suitability for particular gas spectral properties. (See, for example, [39] and [40].)

The most obvious measurement technique for absorption loss is to use a long wave guide filled with a gas mixture simulating that of a Jupiter model and to measure the power loss along the waveguide when an excitation source at one end sends microwaves down the gaseous channel. However, this technique has been found relatively insensitive and tediously slow with very active gases such as ammonia, primarily because of the non-precise gas accountability when using very large surface-to-volume shape factors for the gas cell.

Assuming the need for metallic channels to withstand pressures simulating the Jupiter atmosphere, it must be remembered that a gas such as ammonia is sufficiently active to combine immediately with, or to be effectively absorbed into, the walls of the measurement

system until saturation levels are reached. Practically, this means that even in a relatively compact system, long after all the valves for admitting a given small quantity of ammonia are closed, the pressure gauge at the measurement cell will continue to drop in indicated pressure, as the ammonia gas is absorbed into the walls of the measurement apparatus. Particularly in the case of very long shock tubes, one may envision hours, or even days, of waiting for a stable condition to ensue for each substantial change of ammonia partial pressure or abundance, unless the measurements can somehow be scaled to a more satisfactory range of equipment sensitivity.

Relying heavily on the experience and recommendations of Dr. A. A. Maryott of the National Bureau of Standards (NBS) and using his established facilities under an ARC-NBS interagency arrangement, difficulties of the above types have been mitigated (but by no means removed) by a much more sensitive resonant-cavity and swept-frequency technique. By this technique, changes in power transmitted through the cavity are observed while varying proportions of hydrogen, helium and ammonia are admitted to the cavity. With a cavity having a quality factor Q = 40,000 and with all measurements made over the same cellular space, this technique has many sensitivity and accuracy advantages over waveguide methods.

A greatly simplified diagram of the measurement-test layout is shown in figure 10. Not shown are the multiplicities of coarse and vernier control gas valves, close-off and isolation valves, coarse and

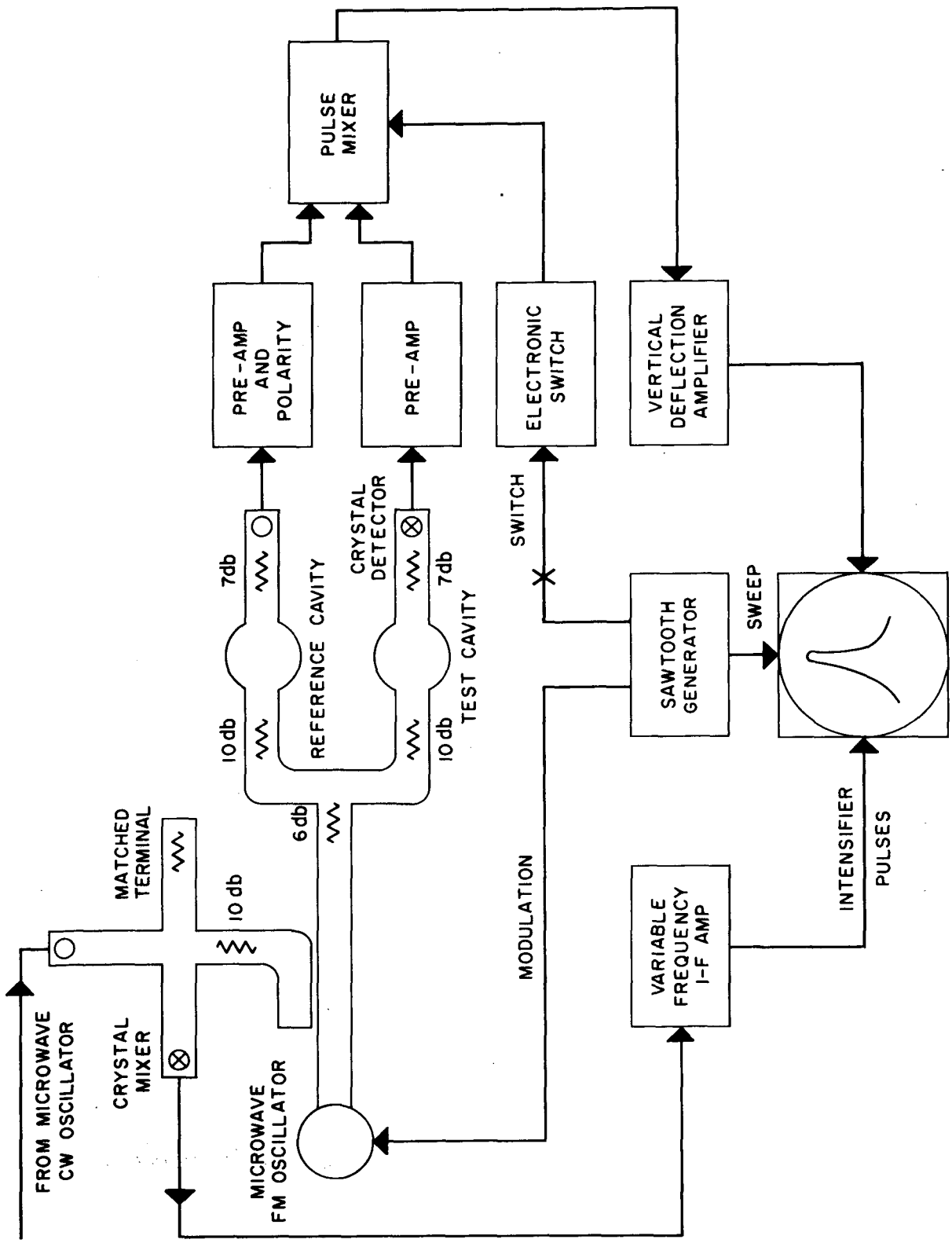

Fig. 10. Basic schematic for measurement of absorption losses.

fine pressure gauges (for all of the different gas inputs), frequency meters, vacuum pumps, warming oven, cooling chamber, tuning stubs, attenuators, microwave controls, power source, thermometers, amplifiers, and reference receiver.

Even with the cavity system, procedural techniques must give maximum attention to ammonia stabilization preparatory to measurement. Since the resonant cavity (about 10 inches in outer diameter for S-band) has a tuning-disk plate that falls just short of touching the cylindrical wall of the cavity, care must be taken that the chamber walls behind the plate are included in the absorption-saturation stabilization which must be established before the true ammonia abundance in the cavity can be identified. Generally, this requires admission of the ammonia gas into the cavity first.

Despite the much greater sensitivity of the resonant-cavity technique, the typical 1 or 2 torr of ammonia partial pressure that would apply to a Jovian atmosphere model, corresponding to the top cloud level, requires scaling of the ammonia abundance and other partial pressures to the range of maximum sensitivity of the cavity system.

Although the suitability bounds of the resonant-cavity technique are not definite, cavity oscillators, cavity-wave meters, cavity-measurement cells, and waveguide components are generally effective and convenient to use in the region from a few millimeters to about 20-cm wavelength (1.5 GHz). However, it could be quite difficult to provide overlapping measurement cavities for the complete

range of interest, particularly below S-band, because of the limited tuning range of each cavity, especially at the lower frequencies.

It should be noted that the S-band cavity used for most of the measurements in the ARC-NBS tests was tunable over a range of only about 2.3 to 2.6 GHz. As explained previously, however, careful measurements at S-band, coupled with the generally available inversion-line spectral observations at K-band, and very high pressure data at X-band, determine the asymptotically flattened absorption characteristic below S-band quite precisely. That is, establishment of S-band values allows extrapolations below S-band to be made quite accurately, using a modified Van Vleck-Weisskopf spectral curve-shape formulation.

The reference cavity, shown in the diagram of the measurement system, figure 10, provides a frequency reference, for comparison of spectral line shift (generally very small at S-band) under loss-loading conditions. The microwave power is preferably provided by a single-cavity tuned klystron, in this case operating at 2.315 GHz. (Backward wave oscillators and other devices have been tried, but generally with less success, due to noise or stabilization problems.)

The test cavity is operated in a high-Q mode, well separated from other modes. The klystron frequency is swept at a rate of 60 times per second over a range that extends many kHz above and below the cavity resonance frequency (nominally about 61.5 kHz half-power bandwidth when the cavity energy is detected with a crystal [assumed square law] and its output is applied to the vertical deflection plates of a

cathode-ray oscilloscope). The horizontal plates of the oscilloscope are driven by the klystron-frequency-modulator signal.

The cavity-mode curve of power versus frequency is displayed on the screen of the cathode-ray tube. Although power differences can be read from the oscilloscope, calibrated output-ratio attenuators are arranged to allow exactly equivalent readouts to be made from potentiometers by maintaining the oscillographic peak response-trace constant.

8.2 Theory of Measurement

Display of the power-versus-frequency-mode curve by the tuned resonant-cavity method takes place in accordance with the following theory. Let

W = energy stored in the cavity

$\frac{dW}{dt}$ = rate of energy loss or decay

ν = operating frequency of cavity.

By definition, the quality factor Q of the cavity is

$$Q = \frac{\omega W}{dW/dt} = \frac{2\pi\nu W}{dW/dt}$$

where $\omega = 2\pi\nu$. A similar relationship applies to the Q of the gas alone. Also, by definition, the minimum detectable absorption coefficient of the gas, α, expressed as absorption per incremental propagation-path distance is

$$\alpha = \frac{1}{W} \cdot \frac{dW}{dx} = \frac{1}{W} \cdot \frac{dW}{dt} \cdot \frac{dt}{dx}$$

But

$$\frac{dx}{dt} = \text{velocity of electromagnetic wave} = c = \lambda\nu$$

where λ = wavelength and ν = frequency. Hence,

$$\alpha = \frac{1}{W} \cdot \frac{dW}{dt} \cdot \frac{1}{c} = \frac{1}{W} \cdot \frac{dW}{dt} \cdot \frac{1}{\lambda \nu}$$

or

$$\nu = \frac{1}{W} \cdot \frac{dW}{dt} \cdot \frac{1}{\lambda \alpha}$$

from which, using the same Q-relationship for the gas as for the cavity,

$$Q_g = \frac{2\pi\nu W}{dW/dt} = \frac{2\pi W}{dW/dt} \cdot \frac{1}{W} \cdot \frac{dW}{dt} \cdot \frac{1}{\lambda\alpha} = \frac{2\pi}{\lambda\alpha}$$

Let Q_o = effective value of cavity-Q before admitting gas

Q_1 = effective value of cavity-Q after admitting gas;

then

$$\frac{1}{Q_1} = \frac{1}{Q_o} + \frac{1}{Q_g} = \frac{1}{Q_o} + \frac{\lambda\alpha}{2\pi}$$

and rearranging,

$$\alpha = \frac{2\pi}{\lambda} \left(\frac{1}{Q_1} - \frac{1}{Q_o} \right)$$

More sensitive measurements can be obtained by measuring the power registered by a loosely-coupled crystal detector at the peak of the cavity-response curve with and without gas. Under these conditions

$$\frac{Q_1}{Q_o} = \left(\frac{P_1}{P_o} \right)^{1/2}$$

where P_1 and P_o are the peak power-amplitude response of the resonance curves with and without gas, respectively, in the cavity. Substituting in the above equation for Q_g in terms of Q_1,

$$\alpha = \frac{2\pi}{\lambda Q_1} \left[1 - \left(\frac{P_1}{P_o}\right)^{1/2}\right] \tag{8-1}$$

or, in terms of Q_o,

$$\alpha = \frac{2\pi}{\lambda Q_o} \left[\left(\frac{P_o}{P_1}\right)^{1/2} - 1\right] = \frac{\omega}{cQ_o} \left[\left(\frac{P_o}{P_1}\right)^{1/2} - 1\right] \tag{8-2}$$

By measuring the height of the power-versus-frequency-mode curve with ($\alpha \neq 0$) and without ($\alpha = 0$) the absorbing gas in the cavity, and taking $\omega = \omega_o$ for the empty condition, one obtains

$$\frac{\alpha c}{\omega_o} = \frac{1}{Q_o} \left[\left(\frac{U_o}{U}\right)^{1/2} - 1\right] \tag{8-3}$$

where U_o is the height of the response-power curve when $\alpha = 0$, U is the height when $\alpha \neq 0$, and $\omega_o = 2\pi \nu_o$.
For the empty cavity, the quality factor Q_o was found to be approximately 37,600.

8.3 Measurements

In a typical experiment, 100 torr of NH_3 were admitted to the cavity and the height of the power-versus-frequency-mode curve was measured. The foreign gas (H_2, He, or mixture of the two) was then admitted and the height remeasured for each of a series of pressures. This gave the heights ratio U_o/U for each pressure. ω_o and Q_o were determined, and α was computed according to (8-3). All room-temperature measurements were performed at 25.9 $\pm$ 0.5°C. The results for four such experiments, two with hydrogen and two with helium, are shown in figures 11, 12, 13, and 14. In each case, the smooth curve is a least-squares fit. Five runs were made with pure NH_3, eleven with H_2, seven with He and one with H_2+He. Experiments were performed with 50, 100, and 300 torr of NH_3. In all cases the results agreed with the adopted trace-curve formulation within the experimental error. All data were analyzed by fitting them with Eq. (4-7).

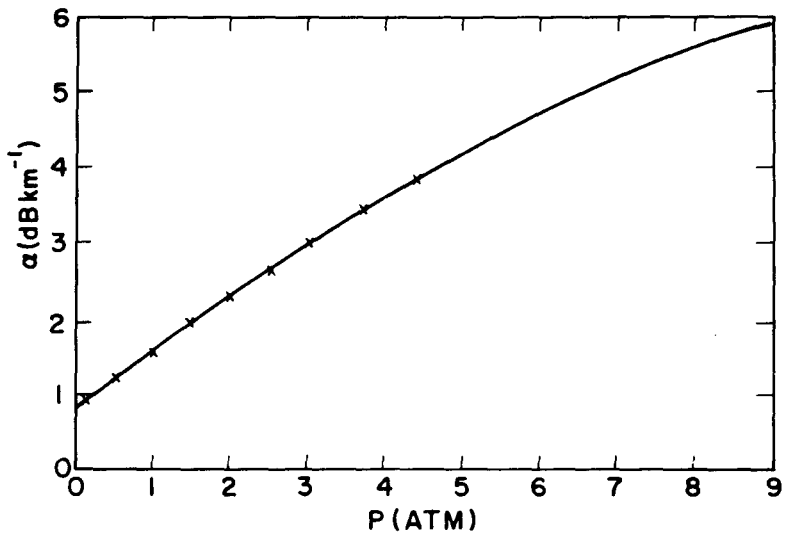

Fig. 11. Absorption coefficient versus pressure for 100 torr of NH_3 broadened by H_2 (2.315 GHz).

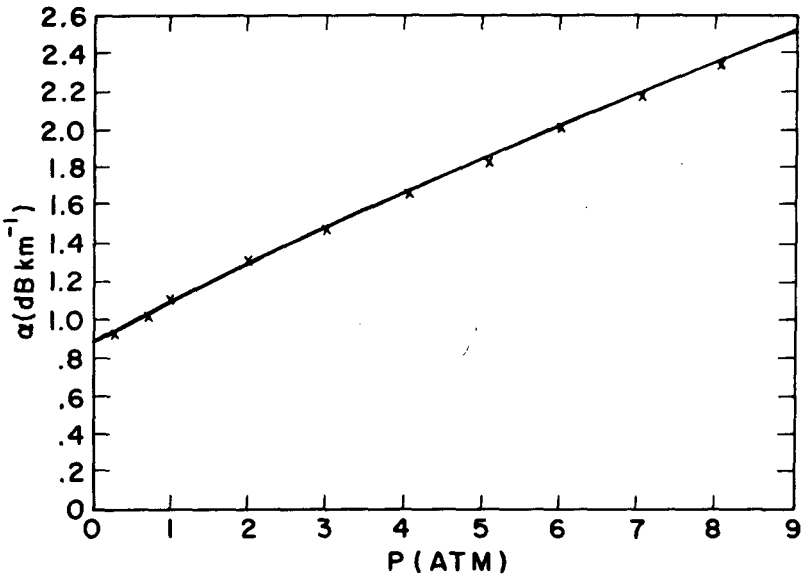

Fig. 12. Absorption coefficient versus pressure for 100 torr of NH_3 broadened by He (2.315 GHz).

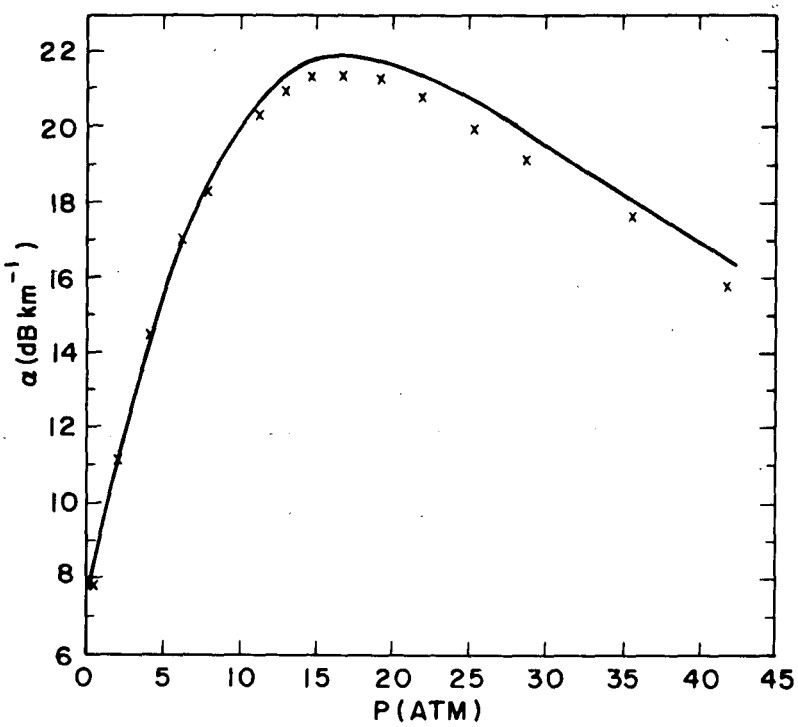

Fig. 13. Absorption coefficient versus pressure for 300 torr of NH_3 broadened by H_2 (2.315 GHz).

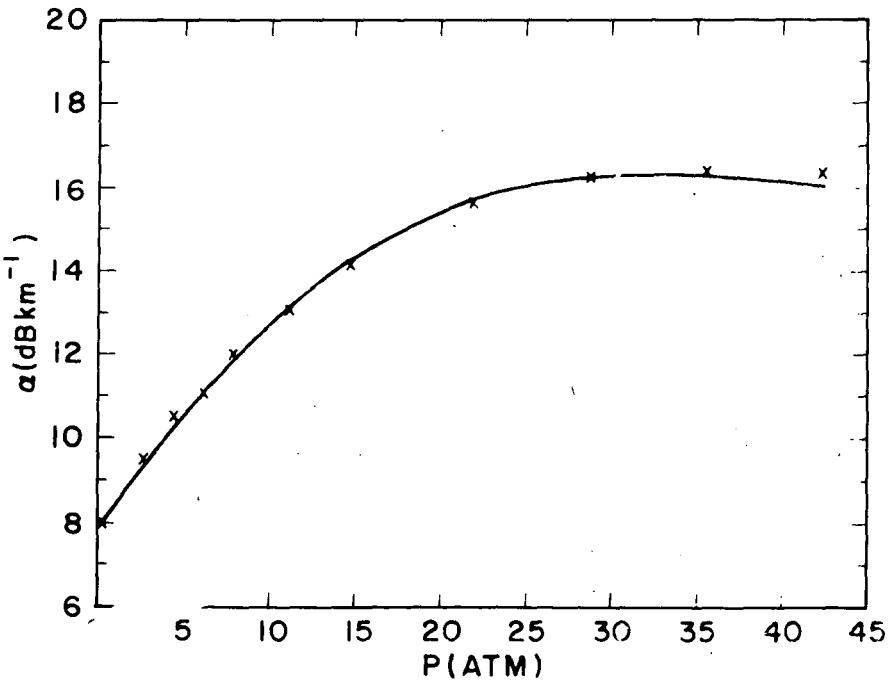

Fig. 14. Absorption coefficient versus pressure for 300 torr of NH_3 broadened by He (2.315 GHz).

In the parameter-range of interest, the gross properties of Eq. (4-10) can be obtained by assuming that the frequency ν of the illuminating wave is nearly zero. Also, for low pressures, the collision frequency γ (proportional to pressure) and the coupling element (frequency) ζ (also proportional to pressure) are both much smaller than the resonance frequency ν_0. Thus, as mentioned in Section 4, Eq. (4-12), Ben-Reuven's shape factor is approximately

$$\mathcal{F} \cong \frac{2(\gamma + \zeta)}{\nu_0^2}$$

where

$$\gamma = aP \quad \text{and} \quad \zeta = bP$$

and P is the pressure. Therefore, the limiting slopes in figures 11 and 12 give a+b. One can do somewhat better than this since it is clear that deviations from linear behavior occur in nature. However, the deviations are not large, so a+b will be more precise than a or b separately. A computer least-squares analysis was carried out in which values of a and b were chosen and the absorption calculated. A "penalty function", PF, was formed which equals the sum of the squares of the differences between the calculated and observed absorption for each data point. The best values of a and b in the

least squares sense were those which minimized PF. In addition, an indication of the possible error was obtained from the expected error in PF. The results are shown in Table 1. In the case of NH_3, the data were sufficient to give only a+b without separation. Therefore, b/a = 0.655 was taken from Ben-Reuven [10], and our value of a+b was utilized to obtain a and b.

For He, a and b could be separated only at high pressures where the use of average values of γ and ζ is not expected to be as accurate. However, similar calculations made with H_2, where a and b could be separated, give results that agree to within the experimental precision. Also note that in figure 12 (and figure 15) better fits to the data were obtained with a_{He} = 0.7 MHz·torr^{-1} and b_{He} = 0.3 MHz·torr^{-1}. These values were used in computing the points plotted in figure 9.

The parameters a and b in Table 1 are valid for a temperature of 300°K and for all but very high pressures, the constraints of which are being analyzed under Phase III studies.

TABLE 1

Gas	a(MHz·torr^{-1})	b	a+b
NH_3	21.4	14.1	35.5 ± 4%
H_2	2.5 ± 10%	1.5 ± 16%	4.0 ± 4%
He	(0.8 ± 10%)*	(0.4 ± 10%)*	1.1 ± 10%

*The discrepancy among a, b, and a+b is within the quoted errors.

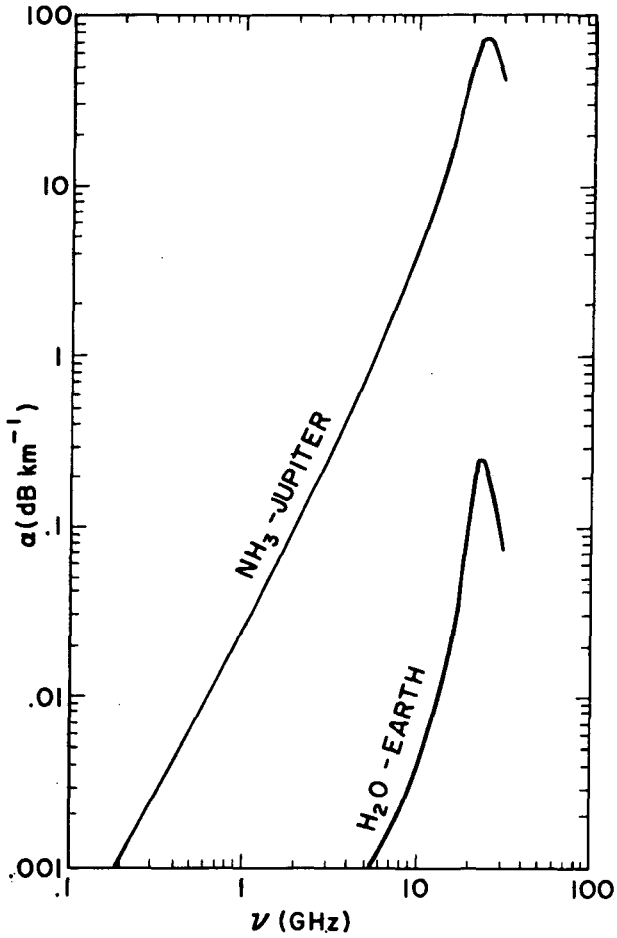

Fig. 9. Absorption coefficient α versus frequency ν at the Jovian cloud top. $P_{H_2} = 2$ atm, $P_{He} = 1.4$ atm, $P_{NH_3} = 2$ torr, $T = 170°K$. For comparison, the absorption due to a mixture of water vapor in air for a typical earth day is shown. The water vapor partial pressure is about 9 torr.

8.4 Jovian Mixtures

To show that the results already cited agree for gas mixtures such as those found on Jupiter, an experiment was performed with NH_3 pressure-broadened by H_2 and He. The only other important constituent of the atmosphere (methane) is far too dilute to affect the NH_3 absorption. The result is shown in Fig. 15. The smooth curve was calculated using the parameters in Table 1, and taking

$$\gamma = (aP)_{NH_3} + (aP)_{H_2} + (aP)_{He}$$

$$\zeta = (bP)_{NH_3} + (bP)_{H_2} + (bP)_{He} \qquad (8\text{-}4)$$

where the P's are partial pressures. There is very good agreement, which means that any Jovian mixture can be treated in the same way, namely by considering each broadening gas separately.

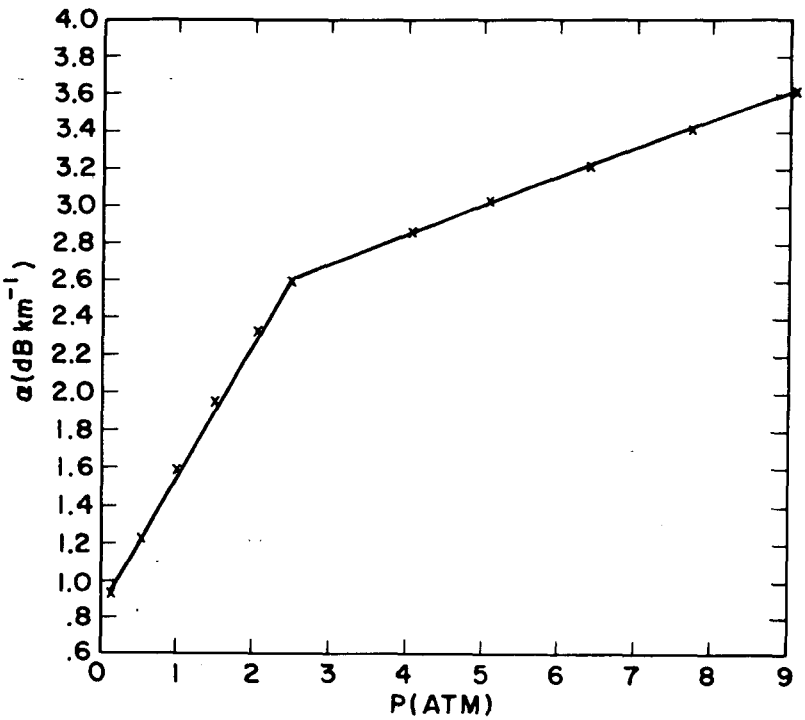

Fig. 15. Absorption coefficient versus pressure for 100 torr of NH_3 broadened by H_2 to 2.49 atm followed by He.

8.5 Temperature Dependence

Another important property is the temperature dependence of the absorption. Referring to Eq. (4-7), it can be seen that there is an explicit T^{-1} dependence, a possible temperature dependence in the sum $\sum_{ij} f_i \left|\mu_{ij}\right|^2$, and a possible temperature dependence in γ and ζ. The absorption coefficient was measured at three temperatures: 25.9°C, 63.9°C, and 115°C. In analyzing these data, the sum $\sum_{ij} f_i \left|\mu_{ij}\right|^2$ was assumed constant and the quantities a and b were determined as previously. These results are shown in figures 16a, 16b, and 16c (which are not to scale). For pure NH_3, $a_{NH_3} + b_{NH_3}$ was proportional to T^{-1} as had been found previously [12]. However, this is difficult to establish with great precision because the temperature range available was rather small. Therefore, in computing the coefficients a and b for H_2 and He, the ammonia coefficients were taken strictly proportional to T^{-1}. The hydrogen coefficients were found to be proportional to $T^{-0.6}$ and the helium coefficients proportional to $T^{-0.7}$. The absorption at Jovian temperatures was calculated on the assumption that these laws hold.

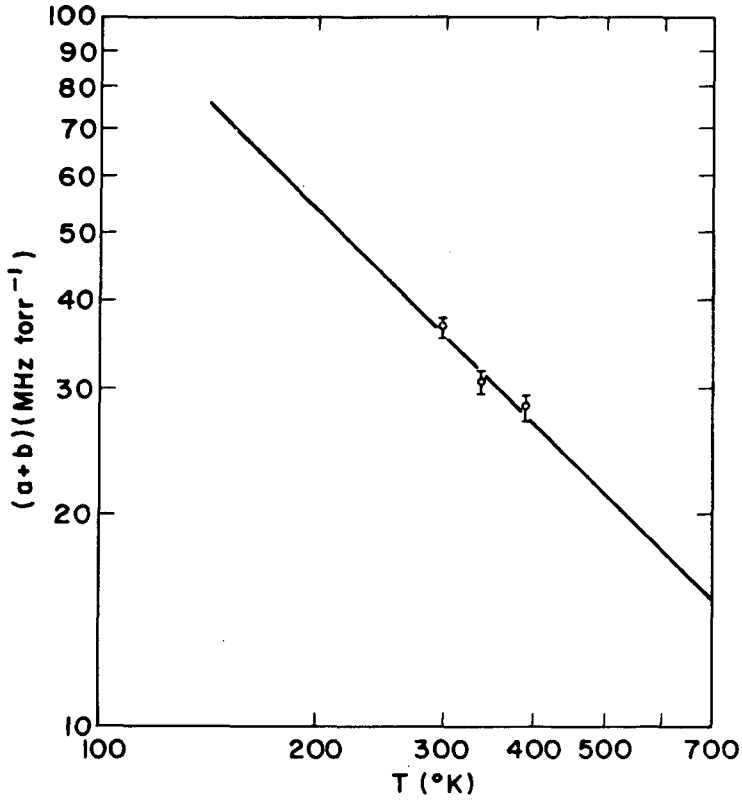

Fig. 16(a). Broadening parameter a+b versus temperature for NH_3.

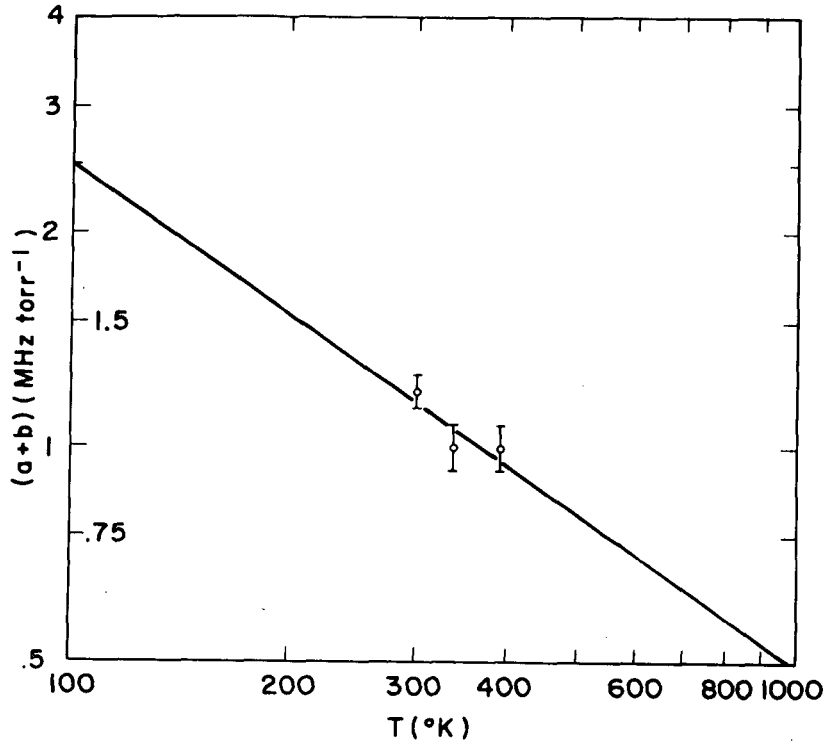

Fig. 16(b). Broadening parameter a+b versus temperature for He.

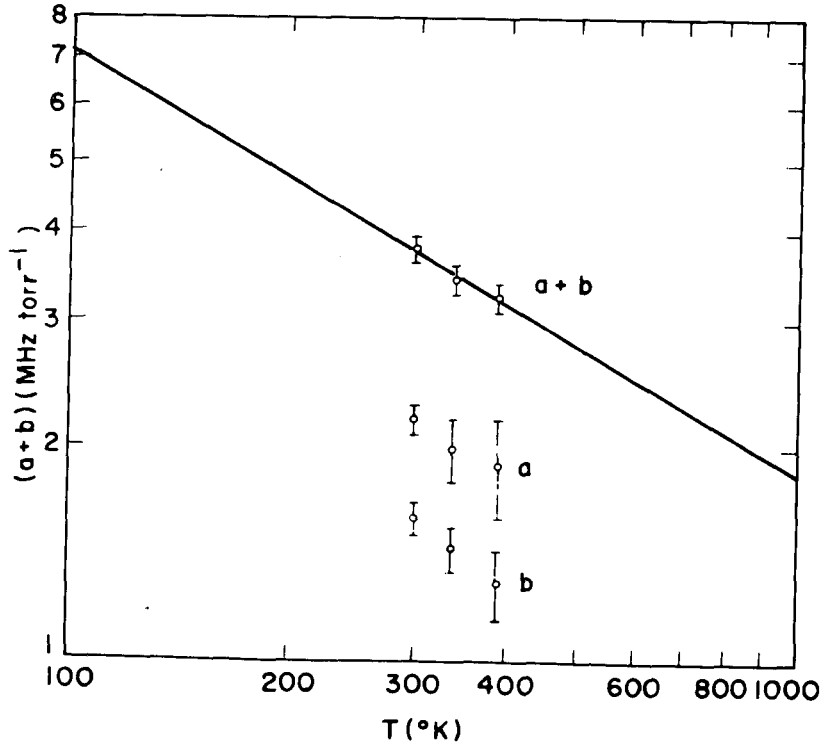

Fig. 16(c). Broadening parameter a+b versus temperature for H_2.

8.6 Other Frequencies

Recently, Morris and Parsons [22] have measured the microwave absorption of ammonia in mixtures of H_2 and He at X-band (9.58 GHz). They were interested primarily in higher pressures and have extended the measurements to several hundred atmospheres. These data were clearly relevant to the Jovian communications problem and were therefore analyzed in the light of the Phase II measurements.

The most obvious method of comparison would be to calculate the absorption at 9.58 GHz using the values of a and b from Table 1 and to compare them with the experimental values. This is shown in Fig. 17. It can be seen that the agreement is quite good for pressures below 25 atm. At the higher pressures there is a discrepancy of about 15% but this is still within the experimental and computational errors of the evaluation technique.

This procedure is not completely valid, however, because of the nature of the averaging implied by Eq. (4-7). In particular, the replacement of $\mathcal{F}_i$ by a common "average" line shape has the disadvantage that averages of combinations of γ and ζ are achieved rather than averages of γ and ζ separately. For example, in the high-pressure, low-frequency limit, the absorption is determined by

$$\sum_{ij} f_i \left|\mu_{ij}\right|^2 \frac{1}{\gamma_i - \zeta_i} \neq \frac{1}{\overline{\gamma_i} - \overline{\zeta_i}} \tag{8-5}$$

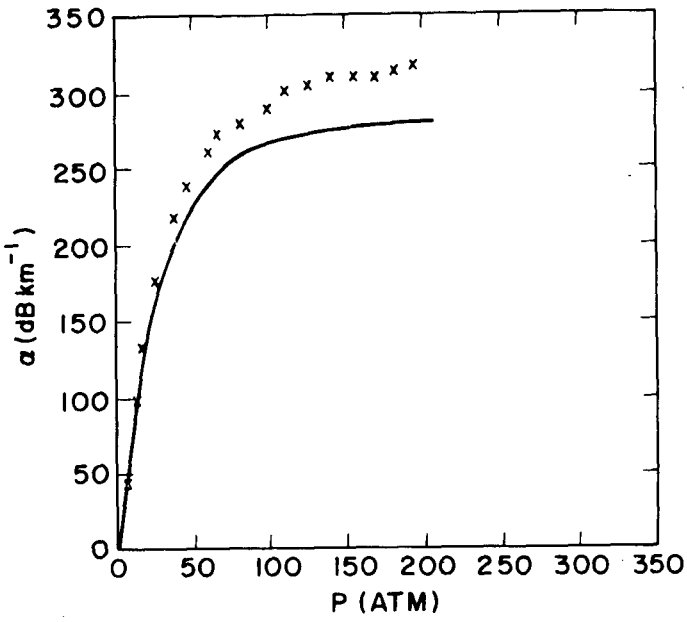

Fig. 17. Absorption coefficient versus pressure for NH_3 plus H_2 in ratio $[NH_3]/[H_2] = 1/128$ (9.58 GHz). Data from Morris and Parson's (22), curve calculated using parameters in Table 1.

Here $\overline{\gamma}_i = \sum_{ij} f_i \left|\mu_{ij}\right|^2 \gamma_i$ and $\overline{\zeta}_i$ similarly. In the low-pressure, low-frequency limit, the absorption is determined by $\sum_{ij} f_i \left|\mu_{ij}\right|^2 (\gamma_i + \zeta_i)$; in this case, one does obtain true average values of γ and ζ. However, the agreement is within the experimental error, so it is sufficiently accurate to use the parameters a and b in this way. The curve of figure 9 was therefore constructed, using these relations and gives the complete frequency dependence for a point near the cloud layer. (Further adjustment of the theoretical formulation, for application to the deeper-atmosphere regions of Jupiter, will be considered under Phase III of the contract.)

9. CALCULATION OF THE AMMONIA - ABSORPTION COEFFICIENT

9.1 Summary of the Procedure

In computing α , one must first find the a's and b's from equations (9-1) (below) using Table 1; then substitute into (8-4) to find γ and ζ ; further, substitute into (4-10) to find α. Figure 18 represents the procedure graphically. This must be done at each point along the path so that the path loss may be evaluated.

This is the procedure used to compute the values of $\alpha(\nu)$ in figure 9, using the particular partial pressures quoted in the figure caption. An example of the computation procedure has been included in this expanded discussion of the Phase-II report.

Symbols and formulae used for computation of the absorption coefficient α as a function of communication frequency ν are:

$$\nu_o = 23{,}400 \text{ MHz}$$

$$\gamma = (aP)_{NH_3} + (aP)_{H_2} + (aP)_{He} \qquad (8\text{-}4)$$

$$\zeta = (bP)_{NH_3} + (bP)_{H_2} + (bP)_{He}$$

for NH_3: $a(T) = a(300°K)\ \frac{300}{T}$

$b(T) = b(300°K)\ \frac{300}{T}$

for H_2: $a(T) = a(300°K)\ (\frac{300}{T})^{0.6}$

$b(T) = b(300°K)\ (\frac{300}{T})^{0.6}$ (9-1)

for He: $a(T) = a(300°K)\ (\frac{300}{T})^{0.7}$

$b(T) = b(300°K)\ (\frac{300}{T})^{0.7}$

The values of the a's and b's at 300°K are given in Table 1 of Section 8.

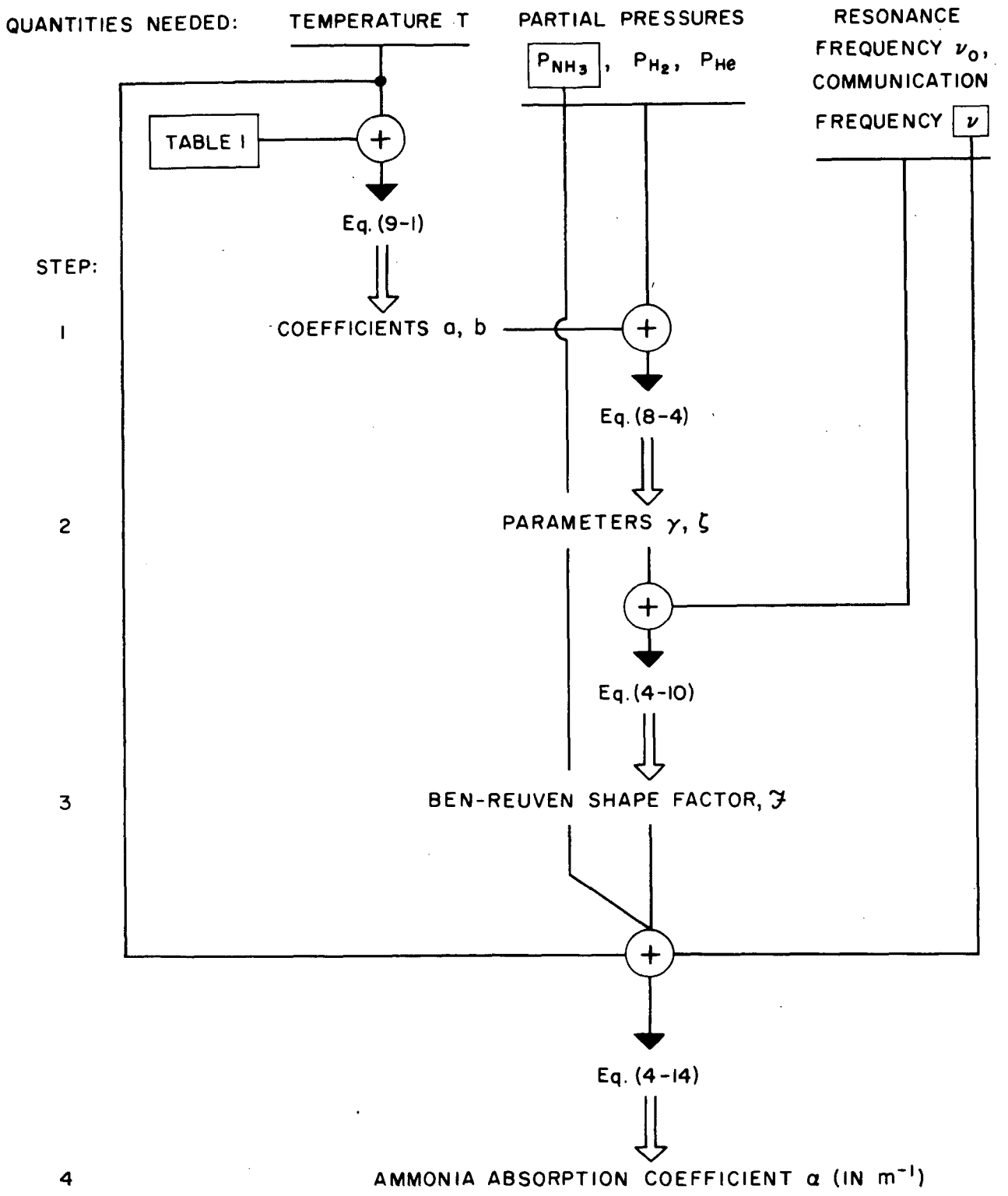

Fig. 18. Procedure for calculating the absorption coefficient α; ↓ means "substitute into," ⇓ means "the result is."

9.2 Sample Calculations

As an example, we will calculate the absorption coefficient α approximately by using the above results. The parameters are as follows (same as for figure 9):

$T = 170°K$

$P_{NH_3} = 2$ torr

$P_{H_2} = 2$ atm $= 1520$ torr (1 atm = 760 torr)

$P_{He} = 1.4$ atm $= 1064$ torr

$\nu_o = 23{,}400$ MHz

$\nu = 2{,}300$ MHz

From Eq. (9-1) and Table 1 of Section 8:

for NH_3: $a(170°K) = 21.4 \frac{300}{170} = 37.8$ MHz $\cdot$ torr^{-1}

$b(170°K) = 14.1 \frac{200}{170} = 24.9$ MHz $\cdot$ torr^{-1}

for H_2: $a(170°K) = 2.5 (\frac{300}{170})^{0.6} = 3.52$ MHz $\cdot$ torr^{-1}

$b(170°K) = 1.5 (\frac{300}{170})^{0.6} = 2.11$ MHz $\cdot$ torr^{-1}

for He: $a(170°K) = 0.8 (\frac{300}{170})^{0.7} = 1.19$ MHz $\cdot$ torr^{-1}

$b(170°K) = 0.4 (\frac{300}{170})^{0.7} = 0.595$ MHz $\cdot$ torr^{-1}

From Eq. (8-4)

$\gamma = 37.8 \times 2 + 3.52 \times 1520 + 1.19 \times 1064 = 6.692 \times 10^3$ MHz

$\zeta = 24.9 \times 2 + 2.11 \times 1520 + 0.595 \times 1064 = 3.890 \times 10^3$ MHz

The communications frequency (ν = 2.3 GHz) is much less than the spectral line-resonance frequency (ν_o = 23.4 GHz). Furthermore, the frequencies γ and ζ are less than ν_o. From Eq. (4-10)

$$\mathcal{F} \cong \frac{2(\gamma + \zeta)}{\nu_o^2} = 3.86 \times 10^{-5} \text{ MHz}^{-1}$$

Using Eq. (4-14) and $\nu = 2.3 \times 10^3$ MHz,

$$\alpha(\nu) = 2.6 \times 10^{-3} \frac{2}{(170)^2} (2.3 \times 10^3)^2 \, 3.86 \times 10^{-5} \text{ m}^{-1}$$

$$= 3.66 \times 10^{-5} \text{ m}^{-1}$$

or since $\alpha(\text{in dB} \cdot \text{km}^{-1}) = 4.34 \times 10^3 \; \alpha(\text{in m}^{-1})$,

$$\alpha(\nu) = 4.34 \times 10^3 \times 3.66 \times 10^{-5} \text{ dB} \cdot \text{km}^{-1}$$

$$= 0.159 \text{ dB} \cdot \text{km}^{-1} \text{ at 2.3 GHz.}$$

This agrees to within about 10 percent of the value shown in Figure 9 (reproduced from the RCA Phase II Final Report, Contract NAS2-5310).

10. TOTAL MICROWAVE ABSORPTION DUE TO AMMONIA

10.1 Power Loss

From the point of view of communications, microwave absorption by gases along the path between transmitter and receiver is very important. In the case of Jupiter and other outer-planet environments, this type of loss is one of the fundamental limitations on a communications system and the absorption-loss variation with frequency is an important design parameter.

In the presence of an absorber the power in an electromagnetic wave will decay exponentially along the path. Consider an electromagnetic wave propagating along a path in the atmosphere in the +x direction. Since the atmosphere is an absorber, the power flow $P(x)$ in the wave will decay along the path according to

$$P(x) = P(0)\, e^{-\alpha x}, \quad x \geq 0 \tag{10-1}$$

where $P(0) = P(x=0)$ is the power flow at the transmitter and α is the spatial rate of decay, or the absorption coefficient. Also, since $P \propto E^2$, the electric field strength is

$$E(x) = E(0)\, \exp(\tfrac{\alpha}{2} x), \quad x \geq 0. \tag{10-2}$$

The absorption coefficient α depends on frequency ν; that is, $\alpha = \alpha(\nu)$, in accordance with the experimentally obtained spectrum and the theoretical formulation. In planetary applications, α depends also on the path length x; that is, $\alpha = \alpha(x)$ which is short for $\alpha(\nu, x)$.

Then,

$$P(x) = P(0) \exp\left[-\int_0^x \alpha(x')\, dx'\right] \tag{10-3}$$

or, for a path length L, the power flow $P(L)$ in the wave, at an arbitrary point $x = L$, is

$$P(L) = P(0) \exp\left[-\int_0^L \alpha(x)\, dx\right]. \tag{10-4}$$

In mks units, α is expressed in m^{-1}, (i.e., per meter), but for communication-design problems, it is often more convenient to work with $dB \cdot km^{-1}$. The conversion equation is:

$$\alpha\,(\text{in dB} \cdot \text{km}^{-1}) = 4.34 \times 10^3\ \alpha .$$

The total signal loss along a path of length L measured in km is defined by

$$A(\text{in dB}) \triangleq -10 \log_{10} [P(L)/P(0)] = 4.34 \int_0^L \alpha(x)\, dx . \tag{10-5}$$

The minus sign in the definition makes the loss a positive quantity.

Our problem is to calculate $\alpha(x)$ for each point in the atmosphere regions of concern and then to integrate along the various paths of interest (occultation, vertical, etc.) to obtain the total signal loss. For example, in Earth's atmosphere, the absorption due to water vapor at 10 GHz typically amounts to about 0.0025 dB/km. At S-Band it is much lower, about 0.0004 dB/km. As shown below, in the Jovian atmosphere at cloud level, the absorption at S-band is about 0.05 dB/km and at X-band about 0.6 dB/km. The power of a signal passing through the layer will decay according to Eq. (10-4), and the received power is quite sensitive to α . In this report, the absorptive loss which a probe signal would experience will be calculated for certain frequencies and geometries. Various model atmospheres are considered and a model chosen for actual calculations. However, absorption results are presented in a framework which makes them relatively independent of the particular model used. A detailed calculation of the ammonia absorption coefficient was presented in the previous section, illustrating the computation process. This section considers path integration and discusses possible uncertainties in the calculations, including an uncertainty in the super-refractive height, which is dependent on the assumed hydrogen/helium ratio.

10.2 Path Loss

The path loss for a given geometry (occultation, vertical, etc.) can be obtained by performing the integration in equation (10-3). In general this will have to be done numerically; for an estimate, however, certain approximations may be made. For example, if the ammonia vapor is saturated near the cloud layer, the P_{NH_3} varies exponentially with height according to the equation

$$P_{NH_3}(z) = P_o \exp\left\{-23\left[\frac{T_o}{T(z)} - 1\right]\right\} \tag{10-6}$$

where $P_o = P(z = 0)$.

Also, temperature varies as a function of altitude, or

$$T(z) = T_o - \gamma_a z \tag{10-7}$$

where $T_o = T(z = 0)$.

Here z is the vertical height above the clouds. This variation as applied to the ammonia factor is so drastic that for the upper atmosphere, the minor changes in the other variables in the absorption coefficient determination are rendered inconsequential in comparison. Therefore, they are taken to be constants, and the absorption coefficient becomes

$$\alpha(z) \cong \alpha_o \exp\left[-23\left(\frac{T_o}{T_o - \gamma_o z} - 1\right)\right] . \tag{10-8}$$

The quantity α_o is the absorption coefficient at z=0 and is frequency-dependent, in accordance with figure 9. The point z=0 is taken to be the Jovian cloud top, where the temperature T = 170°K may be regarded as conservatively high, as compared with estimates by a number of other (but not all) planetary scientists. With this relationship, the absorption along a path can be written

$$\text{power loss} = 4.34 \times 10^3 \int_0^x \alpha(x')\, dx' \quad \text{dB} \tag{10-9}$$

with α in $\text{dB} \cdot \text{km}^{-1}$.

The total signal loss is given by Eq. (10-5). In evaluating the integral in Eq. (10-5), two different geometries are assumed: occulation and direct, or vertical†. The result can be written

$$A(\text{in dB}) = \alpha(\nu, z)\, L_{\text{eff}} \tag{10-10}$$

where $\alpha(\nu,z)$ is the absorption coefficient at the lowest point on the ray path in $(\text{dB}\cdot\text{km}^{-1})$, and L_{eff} is the effective path length.

Case A. Vertical (or Direct) Geometry (x=z)

Figure (19) shows the situation for this case. The power loss, from (10-9) is given by

$$\text{power loss} = 4.34 \times 10^3\, \alpha_o \int_0^C \exp\left[-23\left(\frac{T_o}{T_o - \gamma_a z} - 1\right)\right] dz \tag{10-11}$$

† Possible paths could also include any arbitrary path, with refractive bending, requiring other geometries.

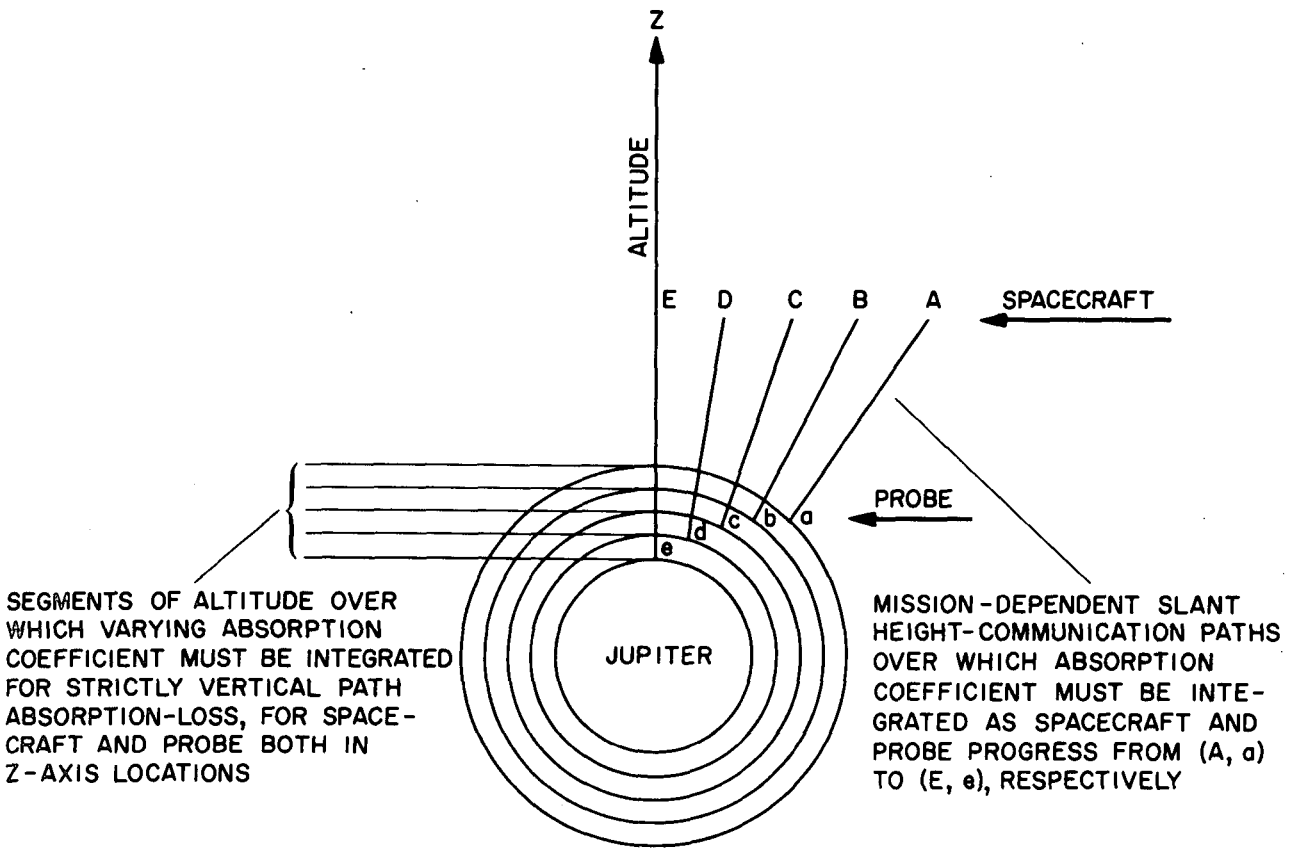

Fig. 19. Direct entry probe-to-spacecraft communication-path absorption loss.

where C is a larger number† that will be specified below. In the region near z=0, where most of the ammonia absorption takes place, $\gamma_a z \ll T_o$. Thus, the following approximation can be made for the exponent in (10-11):

$$23\left(\frac{T_o}{T_o - \gamma_a z} - 1\right) = 23\left[\left(\frac{1}{1 - \gamma_a z/T_o}\right) - 1\right] \cong 23\left[\left(1 + \frac{\gamma_a z}{T_o}\right) - 1\right] \cong \frac{23\,\gamma_a z}{T_o}.$$

With this approximation, the integral in (10-11) becomes

$$\int_0^C \exp\left(-\frac{23\,\gamma_a z}{T_o} z\right) dz \qquad (10\text{-}12)$$

whose value, when $C = \infty$, is $\frac{T_o}{23\,\gamma_a}$. Therefore, the loss is

$$\text{power loss} = 4.34 \times 10^3\, \alpha_o \frac{T_o}{23\,\gamma_a}\ \text{dB}. \qquad (10\text{-}13)$$

In this case, the effective path length

$$L_{eff} = \frac{T_o}{23\,\gamma_a} \cong 3\ \text{km}.$$

Case B. Occultation Geometry

Again the same approximations are made, but now the path is different, as shown in figure 20. The power loss, from (10-9) and analogous to (10-12), is given by

† The constant C is introduced because the integral, with $C = \infty$, is infinite [41].

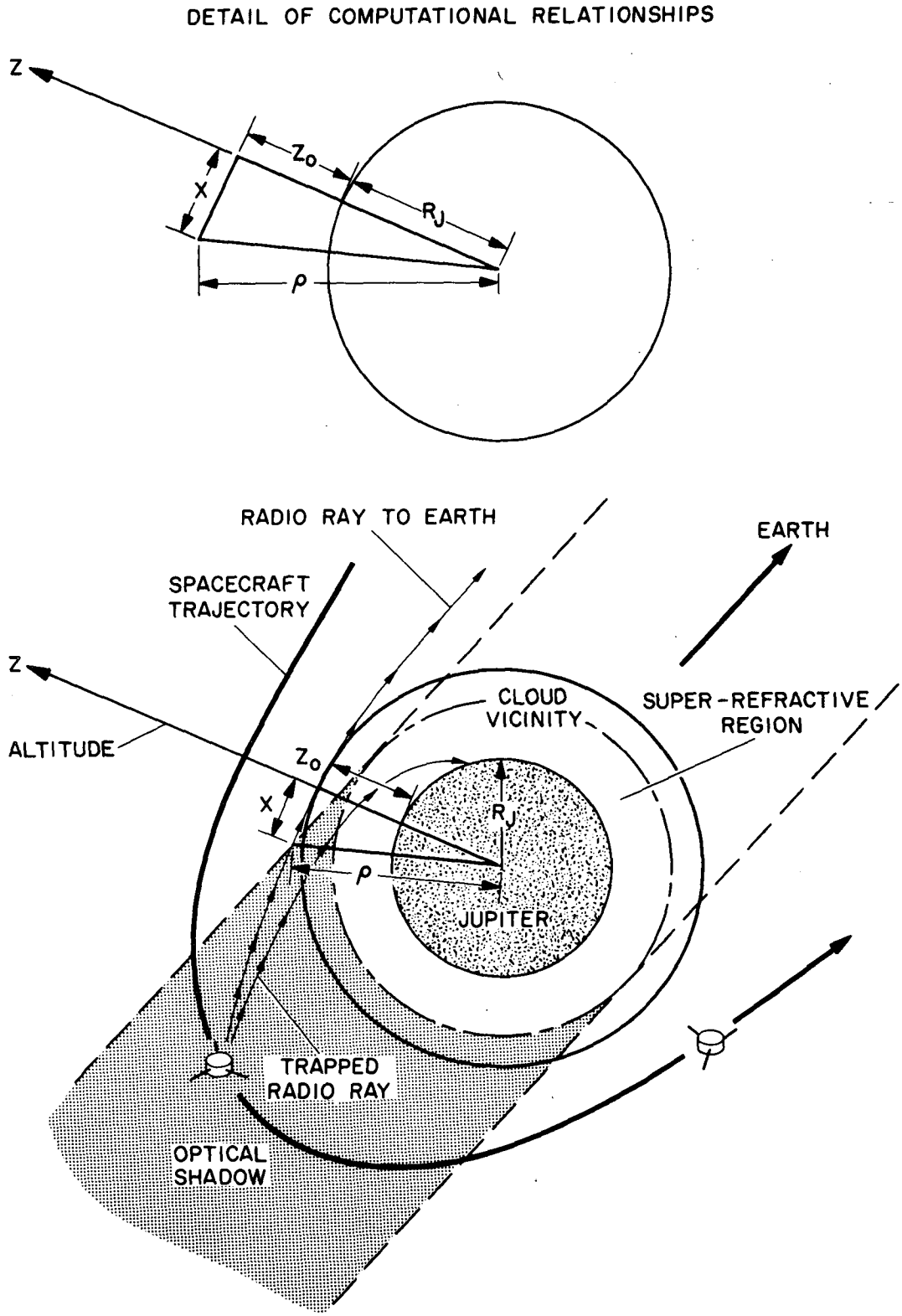

Fig. 20. Occultation mode geometry.

$$\text{power loss} = 4.34 \times 10^{3}\ \alpha_o \int_{x=-C}^{C} \exp\left[-23\,\frac{\gamma_a}{T_o}\,(\rho - R_j)\right] dx \qquad (10\text{-}14)$$

where C again is a large number and

$$\rho = \left[(R_j + z_o)^2 + x^2\right]^{1/2} = (R_j + z_o)\left[1 + \frac{x^2}{(R_j + z_o)^2}\right]^{1/2}$$

from the Pythagorean Theorem. In the region near $x=0$, where most of the absorption occurs, $R_j + z_o \gg x$, so that the following approximation may be made:

$$\rho = (R_j + z_o)\left[1 + \frac{x^2}{(R_j + z_o)^2}\right]^{1/2} \cong (R_j + z_o)\left[1 + \frac{1}{2}\,\frac{x^2}{(R_j + z_o)^2}\right]$$

$$\cong R_j + z_o + \frac{x^2}{2(R_j + z_o)}\ .$$

Then, with $C = \infty$, equation (10-14) reads

$$\text{power loss} = 4.34 \times 10^{3} \alpha_o \exp\ -\frac{23\ \gamma_a\ z_o}{T_o} \int_{-\infty}^{\infty} e^{-Bx^2}\, dx \qquad (10\text{-}15)$$

where we have defined

$$B \triangleq \frac{23\ \gamma_a}{2(R_j + z_o)\ T_o}\ .$$

The integral in (10-15) can be evaluated by recourse to probability theory [41]:

$$\int_{-\infty}^{\infty} e^{-Bx^2}\,dx = \sqrt{2\pi\,(1/2B)}\;\frac{1}{\sqrt{2\pi\,(1/2B)}}\int_{-\infty}^{\infty}\exp\left[-\frac{x^2}{2(1/2B)}\right]dx$$

$$= \sqrt{2\pi\,(1/2B)}$$

if we regard $\dfrac{1}{\sqrt{2\pi(1/2B)}}\exp\left[-\dfrac{x^2}{2(1/2B)}\right]$ as the

probability density function of a random variable that is normally distributed with zero mean and variance 1/2B and use the first axiom of probability theory which, applied here, reads

$$\int_{\substack{\text{whole}\\ \text{range of}\\ \text{definition}\\ \text{of prob. dens.}\\ \text{function}}} (\text{probability density function}) = \text{total probability} = 1.$$

Therefore, equation (10-15) is

$$\text{power loss} = 4.34 \times 10^3\,\alpha_o \exp\left(-\frac{23\,\gamma_a z_o}{T_o}\right)\left[2\pi\,(R_j + z_o)\frac{T_o}{23\,\gamma_a}\right]^{1/2} \qquad (10\text{-}16)$$

$$\cong 4.34 \times 10^3\,\alpha_o\left(2\pi\,R_j\frac{T_o}{23\,\gamma_a}\right)^{1/2}$$

because $\gamma_a z_o / T_o \ll 1$ for values of z_o in figure 20 and $R_j \gg z_o$. The effective path length in this case is

$$L_{eff} = \left(2\pi R_j \frac{T_o}{23 \gamma_a} \right)^{1/2} \cong 1,100 \text{ km.}$$

Taking the absorption coefficient from figure 9 and the effective path as calculated above, we obtain the absorption for the probe at T = 170° K,which is shown in figure 21. Similarly, for an occultation path with $z_o = 0$ (i.e., the ray grazes the cloud tops), one obtains the T = 170°K point on figure 22. In order to construct the complete curves (figures 21 and 22), we again make the assumption [as in equation (10-8)] that only the change in ammonia partial pressure is consequential in significantly changing the absorption in the upper atmosphere of Jupiter. Then

$$\text{power loss} = (\text{power loss at } T = T_o) \exp \left[-23 \left(\frac{T_o}{T_o - \gamma_a z} - 1 \right) \right] \qquad (10\text{-}17)$$

where T_o = 170°K. This is the method used for constructing figures 21 and 22.

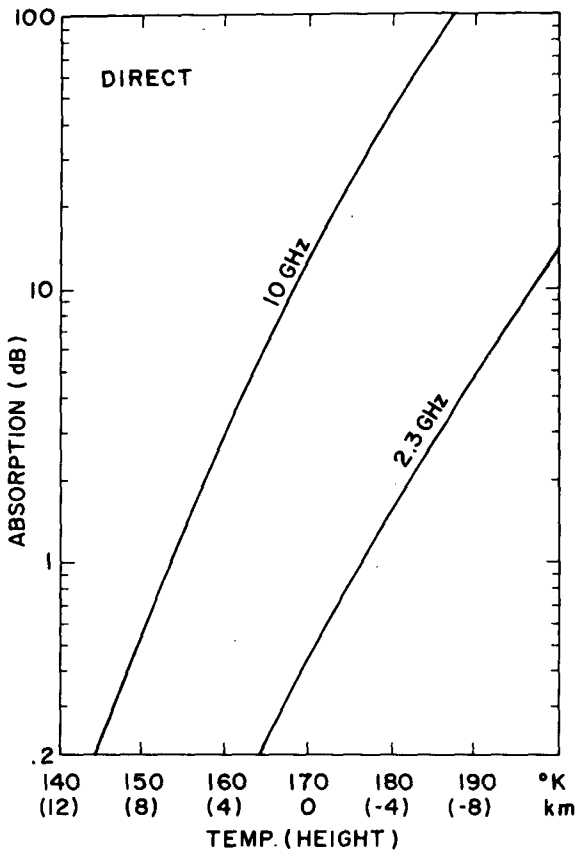

Fig. 22. Total absorption for occultation paths versus temperature at the lowest height probed. In parentheses are the heights above and below the cloud layer which correspond to each temperature according to the model of Moroz.

Fig. 21. Total absorption for direct paths through the atmosphere versus temperature at the probe. In parentheses are the heights above and below the cloud layer which correspond to each temperature according to the model of Moroz.

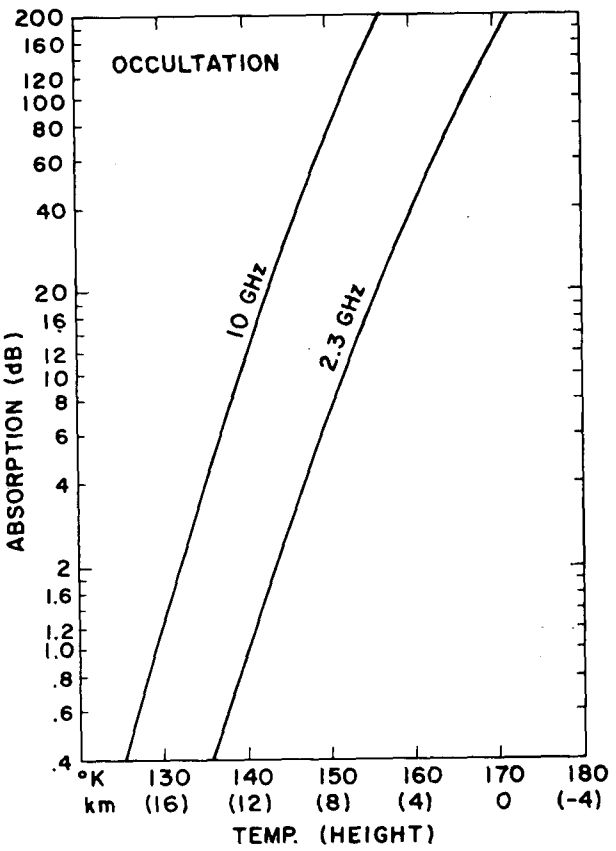

Fig. 21 concerns the direct entry of a probe into the Jupiter atmosphere, and z_o is the distance from the cloud top to the probe. Fig. 22 applies to an occultation experiment (involving transmission from a spacecraft to Earth), and z_o is the distance of closest approach of the transmitted ray from the cloud top. The cloud top is the z=0 reference for the z-axis in the RCA model. Notice that in Eq. (10-8), z may become negative and then measures distances below the cloud level. The results have been plotted primarily as a function of temperature because there is some uncertainty as to the altitude correspondence with temperature at the cloud layer. If a particular model assigns a lower temperature at the cloud top, the abscissa scale should be shifted accordingly. Corresponding values of height according to the model of Moroz [5] are given in the figure. If the Moroz model is followed completely, the cloud-top temperature is 170°K, and the absorption for an occultation experiment is 160 dB at S-band. However, other authors find lower temperatures, e.g., Trafton [6] finds 159°K which implies about 30 dB attenuation. The unfortunate result is that slight uncertainties in temperature produce large uncertainties in signal loss. Apparently, a better model-atmosphere definition will be required to reduce the uncertainty in applying the experimental data to the practical problem of designing a transmitter for use in the Jupiter atmosphere.

The reason for expressing loss in terms of temperature is that temperature is the dominant variable[†]; and to obtain the temperature

---

† J. W. Davenport of RCA advised us, however, in a recent conversation, that it may be more expedient to use pressure as the variable in the loss formulae, for lower atmosphere applications.

that corresponds to a given height requires definitions or assumptions about the model atmosphere. For example, in figures 21 and 22, the Moroz model was used to obtain the distances in km.

10.3 Lowest Point of Signal Penetration

In an occultation experiment, it is of interest to estimate greatest depth of signal penetration. This depends on the power available on the spacecraft as well as on the refractive properties of the atmosphere. For example, the atmosphere may be super-refractive (as with Venus). As illustrated in figure 20, this means that rays parallel to the surface and lower than the super-refractive height are bent into the surface of the planet. The height at which this effect will occur on Jupiter cannot be predicted accurately because the super-refractive height depends critically on the relative proportion of helium -- a quantity which is not definitely known. Fig. 23 shows that the super-refractive height depends critically on the model chosen. The conclusion is qualitatively the same if an adiabatic model atmosphere is used. The critical height is obtained by equating the curvature of the refracted ray with that of the planet. For lower altitudes, the ray curvature will be greater and must therefore intersect the planet. The ray curvature is given by

$$K_r = \frac{1}{n}\left|\frac{\partial n}{\partial z}\right| = \frac{1}{R} \qquad (10\text{-}18)$$

where R is the planetary radius, and n is the refractive index. For an exponential atmosphere,

$$n = 1 + n_o \exp\left(-\frac{z}{h}\right) \text{ and } n_o \ll 1 \qquad (10\text{-}19)$$

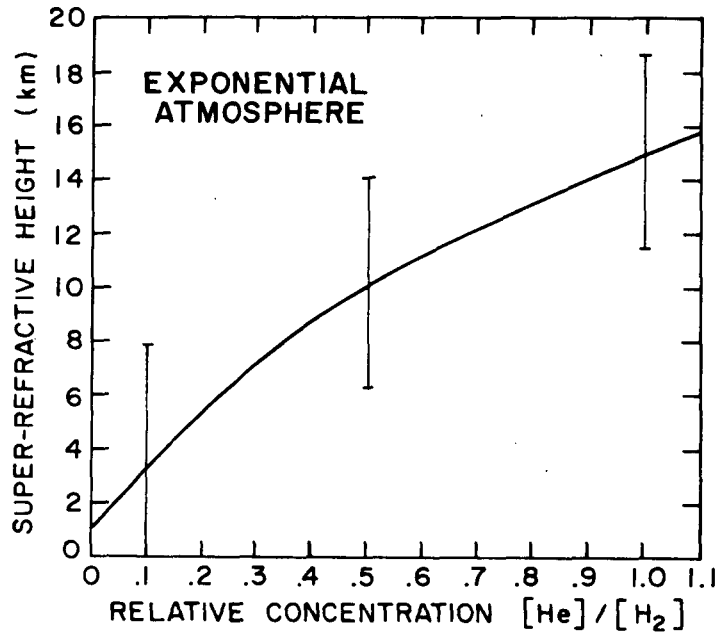

Fig. 23. Super-refractive height versus relative concentration of He. For the Moroz model $[He]/[H_2] = 0.36$.

where n_o is that value of the incremental refractive index at an altitude z equal to the scale height h, which gives the contribution to n of the atmosphere over that of vacuum (for which n = 1). Then

$$\frac{1}{R} \approx \frac{n_o \exp(-z_c/h)}{h} \tag{10-20}$$

which fixes the critical height z_c. Similarly, for an adiabatic atmosphere,

$$n = 1 + n_o \left[\frac{T_o - \gamma_a z}{T_o}\right]^{1/(\gamma-1)} ; \tag{10-21}$$

then

$$\frac{1}{R} \cong \frac{n_o \gamma_a}{T_o (\gamma - 1)} \left[1 - \frac{\gamma_a z_c}{T_o}\right]^{(2-\gamma)/(\gamma-1)} \tag{10-22}$$

which again fixes z_c. However, as indicated previously, the critical height z_c can be said to be only within 10 to 15 km of the cloud layer, depending on the model chosen. Determination of the exact height will have to await a better determination of the helium concentration. If that concentration is relatively low (as in [7]), it may be possible to probe down to the cloud layer with an occultation experiment. This would require sufficient signal power to overcome both refractive defocussing and absorption. The former produces between 20 and 30 dB loss at the cloud layer [14] and the latter about 30 dB, at S-band. Below the cloud layer, the absorption increases much more rapidly than defocussing, so absorption would dominate. Above the cloud layer, the absorption would be the lesser of the two propagation losses.

10.4 Evaluation of the JPL/Lewis Model Atmospheres

As previously indicated evaluation of the absorption loss applicable to the JPL/Lewis model atmospheres is a subject being investigated under Phase III studies, which will be formally reported at a later date. However, it is possible to obtain estimates of the ammonia absorption to a considerable pressure depth using the procedures outlined in this report.

Using the tables of atmospheric definition shown on the following pages, corresponding to JPL's "cool-dense", "nominal," and "warm-extended" atmospheric models, tentative absorption loss-rate variations with change of altitude have been computed, with results as shown in figures 24, 25, and 26 respectively. Integrated vertical (radial) path losses for varying pressure depths of probe entry are shown in figure 27, for the same three atmospheric models, at the 2.3 GHz frequency. Saturation effects are particularly well shown in the "cool-dense" absorption coefficient curves of figure 24.

The following proportional pressures of hydrogen and helium (relative to total pressure P) were used for the respective JPL/Lewis models:

Cool, dense: $P_{H_2} = .68P$, $P_{He} = .31P$

Nominal: $P_{H_2} = .86P$, $P_{He} = .13P$

Warm, extended: $P_{H_2} = .93P$, $P_{He} = .06P$

TABLE 2 (JPL/Lewis)

GAS ABUNDANCE FOR
COOL, DENSE MODEL JUPITER ATMOSPHERE

Z km	T deg K	P atm	P_{NH_3} atm	P_{H_2S} atm	P_{H_2O} atm	P_{CH_4} atm
+25	108	.16	-	-	-	2.3x10-4
+20	108	.24	-	-	-	3.5x10-4
+15	117	.35	-	-	-	4.8x10-4
+10	126	.48	-	-	-	7.0x10-4
+5	135	.70	1.0x10-5	-	-	1.0x10-3
0	144	1.0	6.0x10-5	-	-	1.4x10-3
-5	153	1.3	4.0x10-4	-	-	1.8x10-3
-10	161	1.7	5.0x10-4	-	-	2.4x10-3
-15	169	2.3	6.0x10-4	-	-	3.2x10-3
-20	179	3.0	7.5x10-4	-	-	4.2x10-3
-25	187	3.6	9.3x10-4	1.0x10-5	-	5.2x10-3
-30	196	4.4	1.15x10-3	3.0x10-5	-	6.3x10-3
-35	204	5.3	1.4x10-3	1.0x10-4	-	7.5x10-3
-40	213	6.4	1.8x10-3	3.0x10-4	1.0x10-5	9.0x10-3
-45	222	7.8	2.2x10-3	3.6x10-4	2.8x10-5	1.1x10-2
-50	230	9.5	2.8x10-3	4.6x10-4	9.0x10-5	1.3x10-2
-55	239	11.5	3.5x10-3	6.0x10-4	2.8x10-4	1.5x10-2
-60	248	13.9	4.3x10-3	7.1x10-4	9.0x10-4	1.8x10-2
-65	257	16.8	5.4x10-3	9.0x10-4	1.5x10-3	2.2x10-2
-70	266	20.0	6.6x10-3	1.1x10-3	3.0x10-3	2.6x10-2
-75	275	25.0	8.2x10-3	1.4x10-3	5.5x10-3	3.4x10-2
-80	284	30.0	1.0x10-2	1.8x10-3	1.0x10-2	4.2x10-2
-85	293	36.0	1.2x10-2	2.3x10-3	1.8x10-2	5.3x10-2
-90	302	44.0	1.5x10-2	2.8x10-3	3.3x10-2	6.4x10-2
-95	311	53.0	1.8x10-2	3.4x10-3	6.4x10-2	7.5x10-2
-100	320	65.0	2.2x10-2	4.0x10-3	1.1x10-1	8.6x10-2
-110	329	78.0	2.4x10-2	4.6x10-3	1.7x10-1	9.7x10-2
-120	348	92.0	3.2x10-2	5.3x10-3	1.9x10-1	1.1x10-1
-130	367	108.0	4.0x10-2	6.6x10-3	2.2x10-1	1.3x10-1
-140	385	136.0	5.0x10-2	8.3x10-3	2.8x10-1	1.7x10-1
-150	404	171.0	5.5x10-2	9.1x10-3	3.5x10-1	2.1x10-1
-160	423	215.0	6.7x10-2	1.1x10-2	4.4x10-1	2.6x10-1
-170	441	270.0	8.5x10-2	1.4x10-2	5.5x10-1	3.3x10-1
-175	450	300.0	1.0x10-1	1.6x10-2	6.1x10-1	3.7x10-1
-180	459	333.0	1.1x10-1	1.7x10-2	6.7x10-1	4.1x10-1
-185	468	375.0	1.2x10-1	1.9x10-2	7.5x10-1	4.5x10-1
-190	477	422.0	1.4x10-1	2.2x10-2	8.5x10-1	5.1x10-1
-195	486	471.0	1.6x10-1	2.6x10-2	9.5x10-1	5.7x10-1
-200	495	530.0	1.8x10-1	3.0x10-2	1.1x10-1	6.6x10-1

TABLE 3 (JPL/Lewis)

GAS ABUNDANCE FOR
NOMINAL MODEL JUPITER ATMOSPHERE

Z km	T deg K	P atm	P_{NH_3} atm	P_{H_2S} atm	P_{H_2O} atm	P_{CH_4} atm
+25	125	.30	-	-	-	2.0x10-4
+20	136	.40	1.0x10-5	-	-	3.0x10-4
+15	147	.55	1.0x10-4	-	-	4.0x10-4
+10	158	.70	1.2x10-4	-	-	5.0x10-4
+5	169	.85	1.4x10-4	-	-	6.0x10-4
0	180	1.00	1.7x10-4	1.0x10-5	-	7.0x10-4
-5	191	1.15	1.9x10-4	2.0x10-5	-	8.0x10-4
-10	202	1.30	2.2x10-4	4.4x10-5	-	9.0x10-4
-15	212	1.45	2.5x10-4	5.0x10-5	1.0x10-5	1.0x10-3
-20	223	1.60	2.7x10-4	5.6x10-5	6.0x10-5	1.1x10-3
-25	234	1.80	3.1x10-4	6.2x10-5	2.0x10-4	1.3x10-3
-30	244	2.10	3.6x10-4	7.2x10-5	8.0x10-4	1.5x10-3
-35	255	2.40	4.1x10-4	8.2x10-5	1.5x10-3	1.7x10-3
-40	265	2.80	4.8x10-4	9.6x10-5	2.2x10-3	1.9x10-3
-45	276	3.2	5.4x10-4	1.1x10-4	3.8x10-3	2.2x10-3
-50	286	3.7	6.3x10-4	1.3x10-4	4.5x10-3	2.6x10-3
-55	297	4.3	7.3x10-4	1.5x10-4	5.0x10-3	3.0x10-3
-60	307	5.0	8.5x10-4	1.7x10-4	6.0x10-3	3.5x10-3
-65	317	5.8	9.7x10-4	1.9x10-4	7.0x10-3	4.1x10-3
-70	327	6.6	1.1x10-3	2.1x10-4	8.0x10-3	4.7x10-3
-80	347	8.4	1.4x10-3	2.7x10-4	1.0x10-2	6.0x10-3
-90	366	10.3	1.7x10-3	3.4x10-4	1.2x10-2	7.0x10-3
-100	385	12.0	2.0x10-3	4.0x10-4	1.4x10-2	8.0x10-3
-110	403	14.0	2.3x10-3	4.6x10-4	1.6x10-2	9.0x10-3
-120	421	16.0	2.7x10-3	5.3x10-4	1.9x10-2	1.1x10-2
-130	439	18.0	3.1x10-3	6.0x10-4	2.2x10-2	1.3x10-2

TABLE 4 (JPL/Lewis)

GAS ABUNDANCE FOR

WARM, EXTENDED MODEL JUPITER ATMOSPHERE

Z km	T deg K	P atm	P_{NH_3} atm	P_{H_2S} atm	P_{H_2O} atm	P_{CH_4} atm
+50	120	.20	-	-	-	7.0x10-5
+45	132	.26	1.0x10-5	-	-	9.0x10-5
+40	144	.32	2.7x10-5	-	-	1.1x10-4
+35	155	.39	3.2x10-5	-	-	1.3x10-4
+30	167	.46	3.7x10-5	-	-	1.5x10-4
+25	179	.54	4.3x10-5	3.0x10-6	-	1.7x10-4
+20	191	.62	5.0x10-5	1.0x10-5	-	2.0x10-4
+15	202	.71	5.9x10-5	1.2x10-5	-	2.4x10-4
+10	214	.80	7.0x10-5	1.4x10-5	1.0x10-5	2.8x10-4
+5	226	.90	7.9x10-5	1.6x10-5	6.0x10-5	3.2x10-4
0	238	1.00	8.8x10-5	1.8x10-5	3.0x10-4	3.5x10-4
-5	249	1.11	9.8x10-5	1.9x10-5	6.5x10-4	3.9x10-4
-10	261	1.23	1.1x10-4	2.2x10-5	7.3x10-4	4.3x10-4
-15	273	1.36	1.2x10-4	2.4x10-5	8.1x10-4	4.8x10-4
-20	285	1.51	1.3x10-4	2.7x10-5	9.0x10-4	5.3x10-4
-25	297	1.68	1.5x10-4	3.0x10-5	1.0x10-3	5.9x10-4
-30	309	1.87	1.6x10-4	3.2x10-5	1.1x10-3	6.5x10-4
-35	321	2.08	1.7x10-4	3.5x10-5	1.2x10-3	7.3x10-4
-40	333	2.31	1.9x10-4	3.9x10-5	1.3x10-3	8.1x10-4
-45	345	2.56	2.1x10-4	4.3x10-5	1.4x10-3	8.9x10-4
-50	357	2.82	2.4x10-4	4.8x10-5	1.6x10-3	9.7x10-4
-55	369	3.10	2.6x10-4	5.3x10-5	1.8x10-3	1.0x10-3
-60	381	3.40	2.9x10-4	5.9x10-5	2.0x10-3	1.2x10-3
-65	393	3.72	3.2x10-4	6.5x10-5	2.2x10-3	1.3x10-3
-70	405	4.06	3.5x10-4	7.1x10-5	2.4x10-3	1.4x10-3
-75	417	4.45	3.8x10-4	7.7x10-5	2.6x10-3	1.5x10-3
-80	429	4.87	4.1x10-4	8.2x10-5	2.8x10-3	1.7x10-3

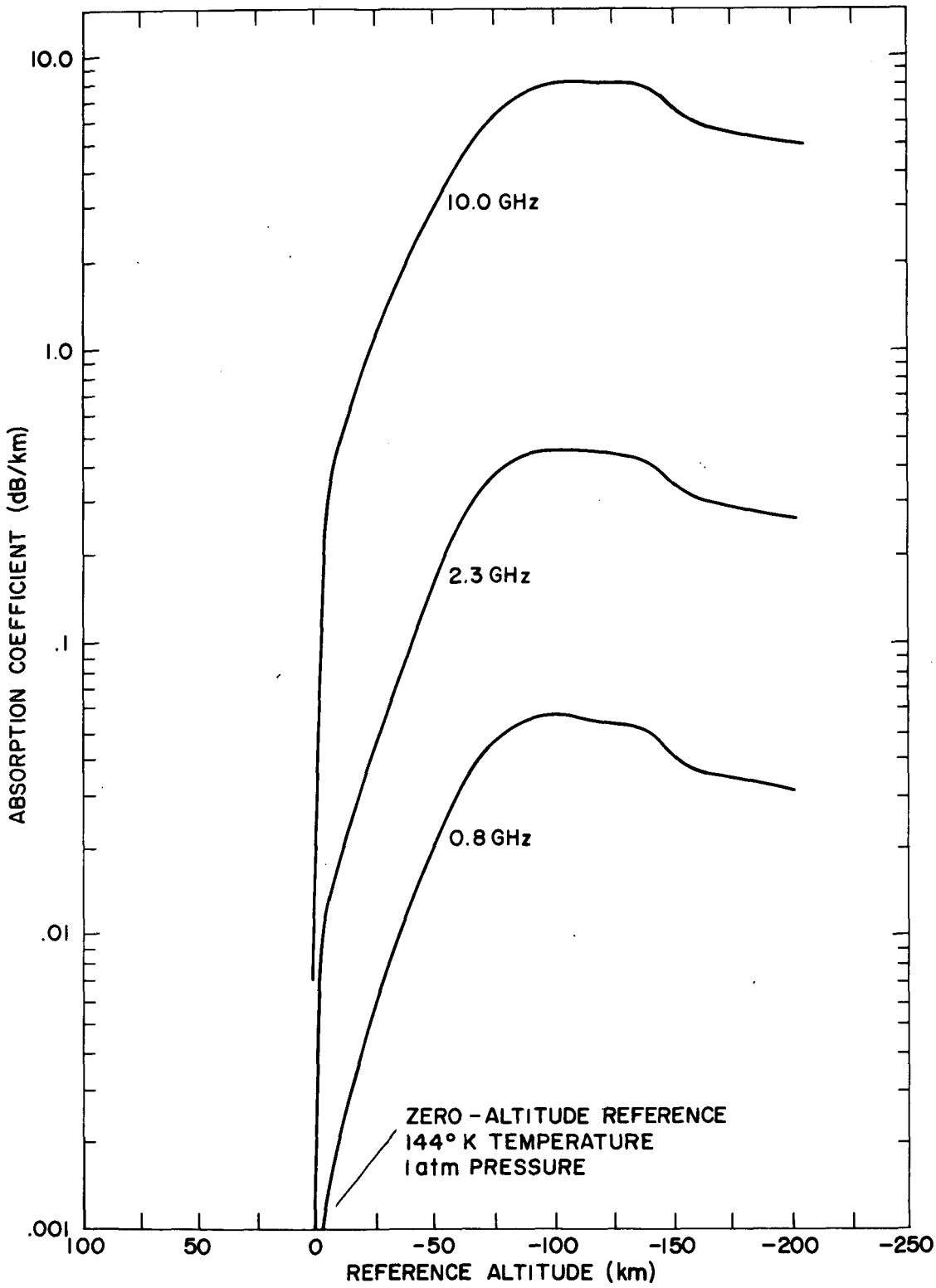

Fig. 24. Cool-dense model (JPL/Lewis).

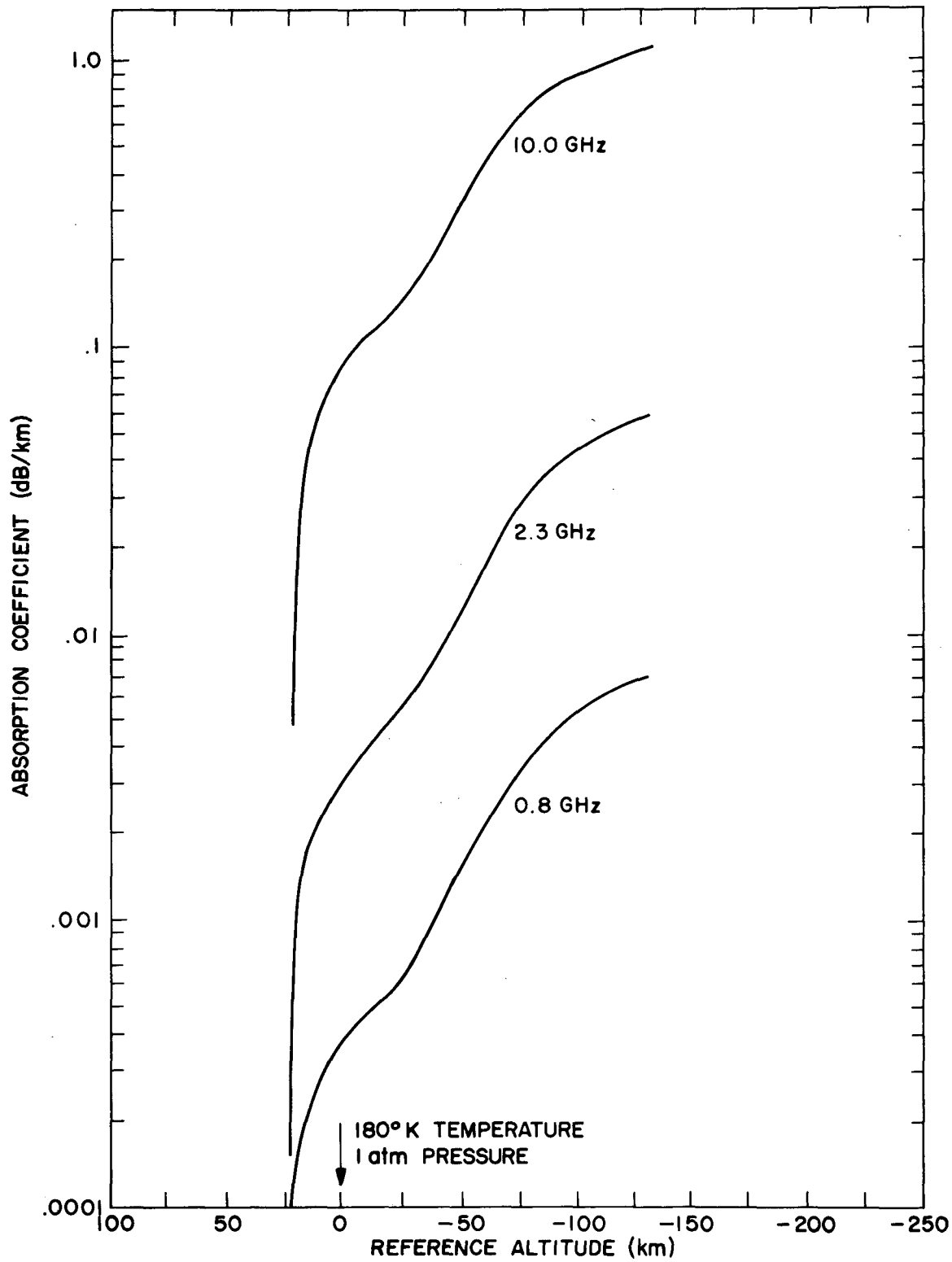

Fig. 25. Nominal model (JPL/Lewis).

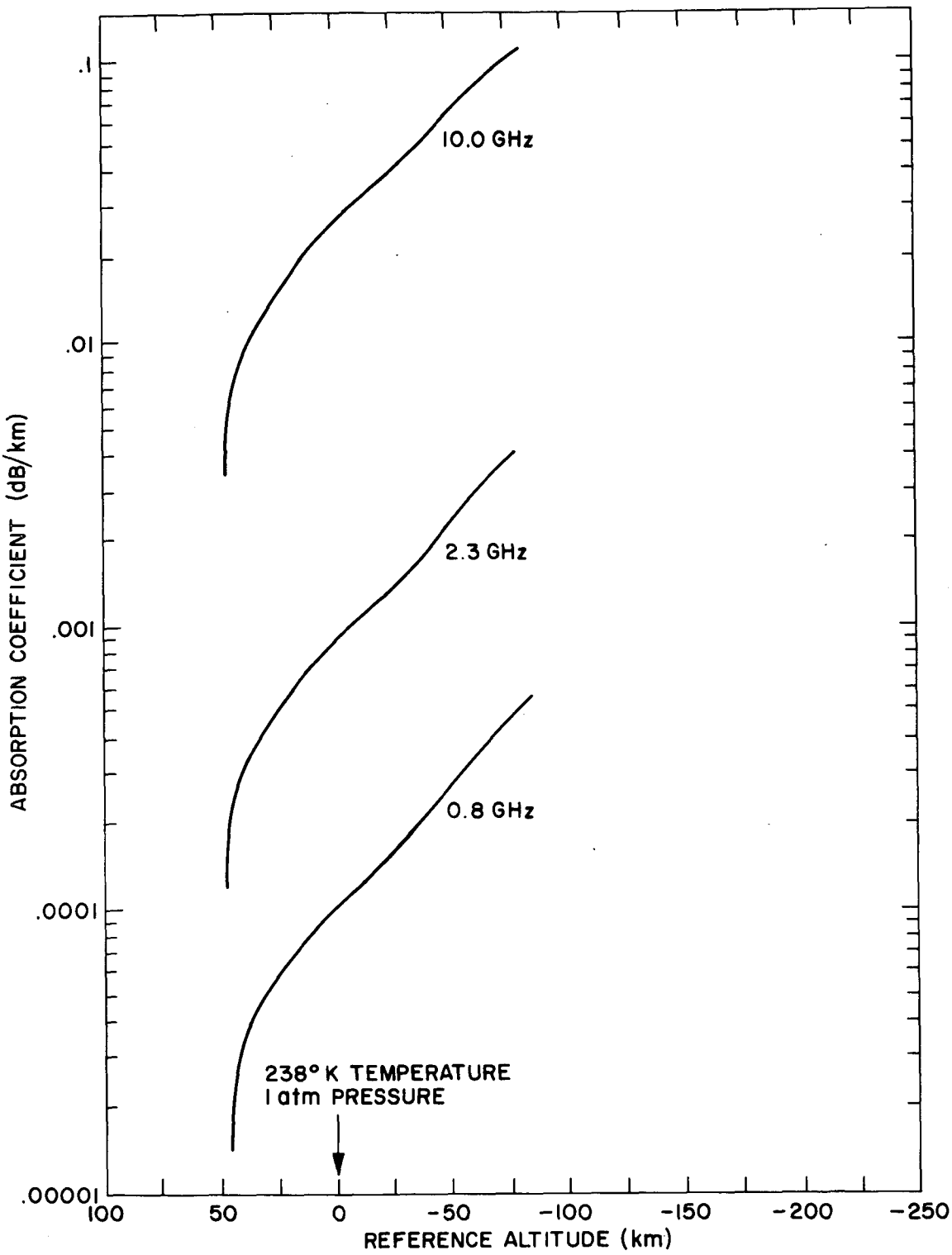

Fig. 26. Warm-extended model (JPL/Lewis).

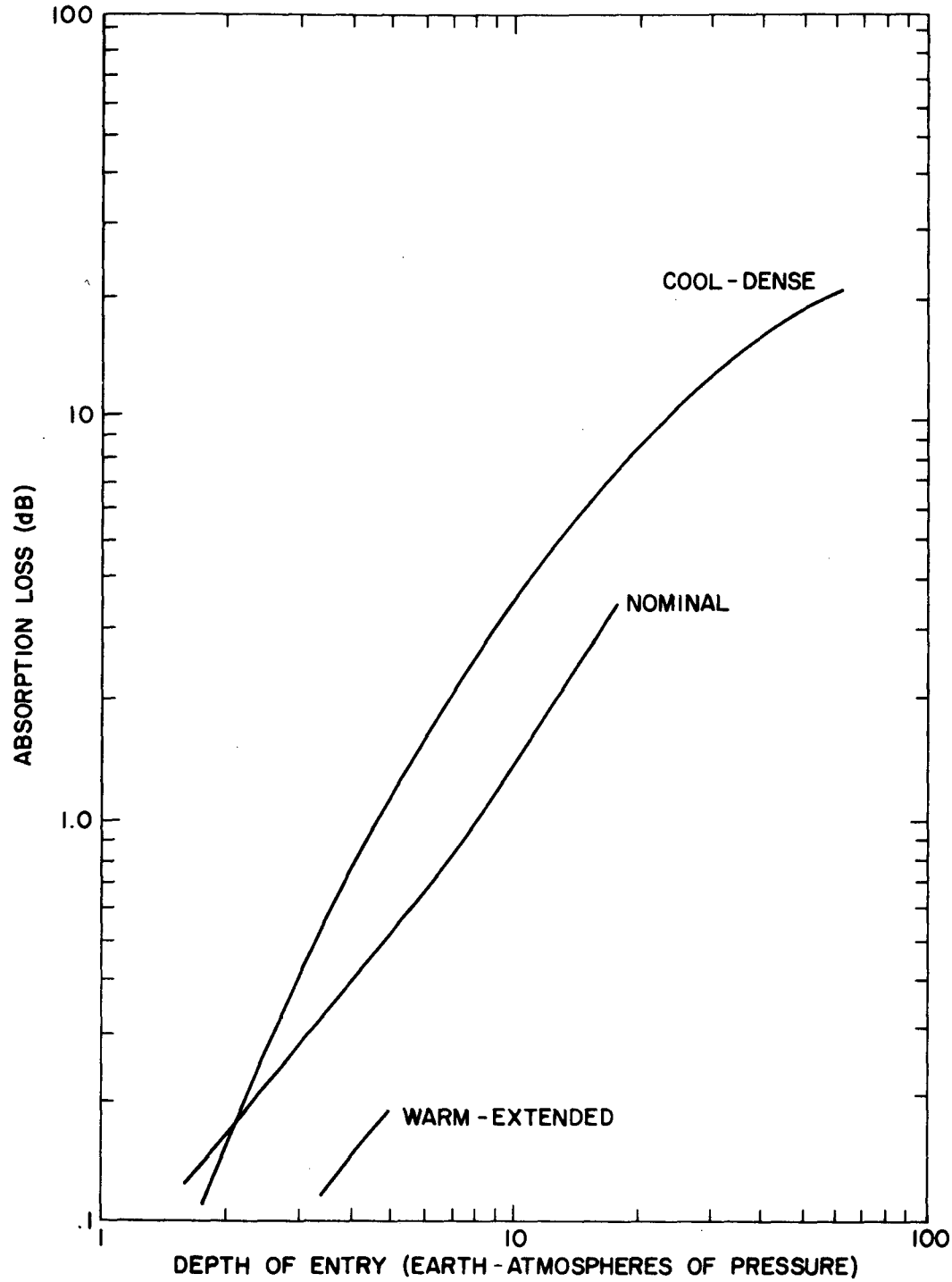

Fig. 27. Integrated absorption loss for vertical entry.

11. GLOSSARY OF TERMS

This glossary of terms is included for completeness and to refresh the reader's memory with the terminology. Many definitions are taken from [43]. Underlined words are defined elsewhere in the glossary.

absorbing molecules	molecules taking energy from a passing electromagnetic wave
absorption coefficient	spatial rate of exponential decay of power flow (a function of excitation frequency) in an electromagnetic wave as it passes through an absorbing medium
absorption spectrum	array of lines and bands resulting from passage of electromagnetic energy through absorbing molecules in a gaseous state
absorptive signal loss	attenuation of an electromagnetic wave due to absorbing molecules
adiabatic atmosphere	model atmosphere in which the atmospheric pressure P decreases with height z as $P \propto (1 - zc)$ where c is a constant of proportionality (dimensions pressure/length)

adiabatic law	states that compression of a gas results in warming, expansion in cooling; formula relating pressure and height in an adiabatic atmosphere
adiabatic-temperature gradient	coefficient in front of the height z in the temperature relationship T = T(z), ratio of gravitational acceleration to specific heat at constant pressure
ammonia-absorption coefficient	absorption coefficient when an electromagnetic wave passes through gas in which ammonia is present
ammonia, saturated	form of ammonia in which its partial pressure equals its vapor pressure; that is, given a fixed volume, no more ammonia molecules can be added
atmospheric composition (or constituency)	types and proportion of molecules present in the atmosphere (often expressed as partial pressures of constituent gases)
atmospheric stability	equilibrium of heat exchange in the atmosphere
atomic inversion	motion of an atom from one position to another within a molecule in a predictable way

atomic orbital wavelength	wavelength of the electromagnetic wave emitted or absorbed when electrons of the atom change from one orbit to another of different energy level
collision broadening	see pressure broadening
collision cross section	area presented by molecules for collision with other molecules
collision frequency	average number of collisions per second between a molecule and ambient molecules present in a gas
collision lifetime	reciprocal of collision frequency
critical height	height from a reference below which an electromagnetic wave is bent onto a path into the planet
defocussing/DSS	weakening of signal as a result of bending of the path of an electromagnetic wave, due to varying density of the propagation medium
diabatic (or nonadiabatic)	with either gain or loss of heat energy
direct geometry	path of an electromagnetic wave whose length within an atmosphere is minimum

effective path length — length of an equivalent path for electromagnetic waves used in power loss calculations

exponential atmosphere — model atmosphere in which the atmospheric pressure P decreases with height z as $P \propto e^{-z/h}$, where h is the scale height having dimensions of length

foreign-body-impact line broadener — type of molecule causing pressure broadening in an absorption spectrum

impact broadening — see pressure broadening

inversion — motion of an atom from one position to another within that molecule to which the atom belongs chemically

inversion atom — atom performing an inversion motion

inversion-line frequency — frequency of that spectral line which is caused by inversion motion of an atom

JPL model atmospheres — three model atmospheres for Jupiter, defined by Neil Divine, called "nominal," "cool, dense," and "warm, extended," each consisting of a table for the gas abundance found at various total pressures (1 atm is taken to be the altitude reference)

K-band	frequency range in the microwave region from 10.9 to 36 GHz (2.75 to 0.834 cm wavelengths), approximately
kilometer-atmosphere	measure of the number of molecules in the atmosphere per unit surface area of the planet; area in a strip under the curve of pressure (in atm) versus altitude (in km) for the planetary atmosphere; for convenience this is converted into the length of the column which would be obtained if the gas were compressed to standard temperature and pressure; for 1 km-atm this length is 1 km
lapse rate	decrease of an atmosphere variable, such as specific heat at constant pressure, as a function of height above a reference
Lewis model atmosphere	model atmosphere of Jupiter proposed by John S. Lewis of the Massachusetts Institute of Technology

line shape theory	theoretical formulation of the experimentally observed variation of the line spectrum with frequency of excitation
line-spectra curve-technique	theoretical prediction of the line spectrum in a frequency interval based on observations in another interval
line spectrum	representation of the discrete distribution of electromagnetic energy as a function of frequency
microwave attenuation	decrease in electromagnetic energy in the microwave region as a function of propagation-path length
model atmosphere	theoretical representation of an atmosphere, giving (i) the amounts of constituent gases at certain heights (or total pressures, or temperatures); (ii) the temperature-pressure relationship; (iii) other relationships such as dependence of refractive index on height above a reference

Moroz ("working") model	model atmosphere constructed from data reported by V. I. Moroz in his "Physics of the Planets"
opacity	cross-sectional area per unit mass for an absorbing molecule
optical depth	limiting depth for successful optical transmission
optically thick layer	part of an atmosphere having an optical depth that is greater than that in another part
partial pressure	pressure exerted by one part (constituent) of a gaseous mixture in the same volume
pressure broadening	widening of a resonance line in a line spectrum due to collisions between molecules in a gaseous state
Q	quality factor: the ratio of stored to dissipated energy, as manifested by the tuned-resonance curve
Raleigh scattering	scattering of electromagnetic radiation by particles that are small compared to the wavelength of the radiation

refractive defocussing	defocussing of an electromagnetic wave due to refraction
response-envelope shaping characteristic	resonant response-curve shape representing relative atomic excitation susceptibility as the frequency is swept between the resonant-line frequency and remote values of frequency
rotational energy levels of a molecule	an additional source of atomic energy absorption due to a molecular rotation mode, as distinct from the inversion line mode
S-band	frequency interval from 1.55 to 5.2 GHz (19.3 to 5.77 cm wavelengths), approximately
scale height	measure of the relationship between density and temperature at any point in an atmosphere; thickness of a homogeneous atmosphere (having a density constant with height) which would give the observed temperature

shape factor	function of the excitation frequency and resonance frequency determining the graphical appearance of the absorption spectrum
stable relative-opacity reference	observation condition at which opacity is sufficiently discrete or non-fluctuating as to provide a desirable reference
standard temperature and pressure (STP)	usually a temperature of 0° Celsius (but also used to designate temperature of 15°Celsius) and 1 standard atmosphere of pressure
stratopause	upper-boundary layer of the stratosphere where the temperature gradient is discontinuous
stratosphere	layer of the atmospheric shell of a planet where the temperature is either constant or increases with height above a reference
super-refraction	refraction by a material interface when the refractive index decreases by more than 1.2×10^{-3} , approximately

super-refractive height	height (measured from a reference) below which refraction by the atmosphere causes rays to be bent into the surface of the planet
supra-stratosphere	layer of atmospheric shell lying above the stratosphere
tropopause	upper-boundary layer of the troposphere and lower-boundary layer of the stratosphere where the temperature gradient is discontinuous
troposphere	layer of the atmospheric shell of a planet where the temperature decreases with height above a reference
X-band	frequency range in the microwave region from 5.2 to 10.9 GHz (5.77 to 2.75 cm wavelengths), approximately

GLOSSARY OF SYMBOLS

A	total signal loss along a path of length L (dB)
a	broadening coefficient, in Table 1 ($MHz \cdot torr^{-1}$)
α	absorption coefficient (m^{-1}, km^{-1}, or $dB \cdot km^{-1}$
B	abbreviation for a mathematical expression
b	broadening coefficient, in Table 1 ($MHz \cdot torr^{-1}$)
C	constant
c	speed of light (3×10^8 $m \cdot sec^{-1}$)
c_p	specific heat at constant pressure and volume (joule $\cdot$ $[kg \cdot °K]^{-1}$)
δ	parameter measuring a shift in resonance frequency (Hz)
$E(x)$	electric field strength ($volts \cdot m^{-1}$)
ε_o	permittivity of free space (8.85×10^{-12} $farad \cdot m^{-1}$)
$\mathcal{F}$	Ben-Reuven shape factor (Hz^{-1})
f_i	fraction of the total number of absorbing molecules per unit volume in the lower state
g	acceleration due to gravity on Jupiter ($m \cdot sec^{-2}$)
γ	frequency of molecular collisions in a gas (Hz); ratio of specific heats at constant pressure and volume
γ_a	adiabatic temperature gradient ($°K \cdot km^{-1}$)
$\overline{\gamma_i}$	average frequency of molecular collisions in a gas (Hz)
h	scale height (km)
k	Boltzmann constant (1.38×10^{-23} $joules \cdot °K^{-1}$)
K_r	ray curvature for super-refraction
L	path length of wave propagation (km)

L_{eff}	effective path length for propagation loss (km)
λ	wavelength of exciting wave (m)
μ	dipole moment (coulomb·m)
N	total number of absorbing molecules per unit volume (m^{-3})
N_s	number of scattering molecules per unit volume (m^{-3})
n	refractive index
n_o	incremental refractive index at an altitude equal to the scale height
ν	frequency of exciting wave (Hz)
ν_o	resonance frequency (Hz)
ω	frequency of exciting wave ($rad \cdot sec^{-1}$)
P	total pressure (atm); partial pressure of the absorbing molecules as subscripted ($newton \cdot m^{-2}$, atm, or torr)
P_o	partial pressure of ammonia at a reference attitude ($newton \cdot m^{-2}$, atm, or torr); peak-power amplitude response of resonance curve without gas in cavity
P_1	peak-power amplitude response of resonance curve with gas in cavity
PF	penalty function (sum of squares of differences between calculated and observed absorption)
P(x)	power flow in a wave ($watt \cdot m^{-2}$)
P(z)	pressure as a function of altitude z above a reference (atm)
Q	quality factor of an empty cavity
Q_g	quality factor of a gas

Q_o	effective value of cavity-Q before admitting gas
Q_1	effective value of cavity-Q after admitting gas
R	planetary radius (km)
R_j	radius of Jupiter (7×10^4 km)
ρ	abbreviation of a mathematical expression
σ	collision cross section (m^2)
T	temperature (°K)
T_o	temperature at a reference altitude (°K)
T(z)	temperature as a function of altitude z above a reference (°K)
τ	mean time between molecular collisions (sec)
U_o	height of response-power curve without gas in cavity
U_1	height of response-power curve with gas in cavity
v	thermal velocity ($m \cdot sec^{-1}$)
W	energy stored in cavity (joule)
x	propagation-distance variable (km)
z	altitude above a reference (km)
z_c	critical height for superrefraction (km)
z_o	height of radio wave above Jupiter's surface (km)
ζ	coupling element in Ben-Reuven shape factor (Hz)
$\overline{\zeta_i}$	average of coupling element in Ben-Reuven shape factor (Hz)

12. REFERENCES

1. J. R. Dickel, J. J. Degioanni, and G. C. Goodman, The Microwave Spectrum of Jupiter, Radio Science 5, 517 (1970).
2. D. D. Thornton and W. J. Welch, 8.35 mm Radio Emission from Jupiter, Icarus 2, 228 (1963).
3. G. C. Goodman, Models of Jupiter's Atmosphere, Ph.D. thesis, University of Illinois, Urbana (1969).
4. C. M. Michaux, Handbook of the Physical Properties of the Planet Jupiter, NASA SP-3031, Douglas Aircraft Company, Inc., Santa Monica, Calif. (1967).
5. V. I. Moroz, Physics of Planets, Tech. Translation NASA TT F-515, Washington, D. C. (1968).
6. L. M. Trafton, Model Atmospheres of the Major Planets, Astrophys. J. 147, 765 (1967).
7. T. Owen, The Atmosphere of Jupiter, Science, 167, 1675 (1970).
8. C. M. Michaux, op. cit., pp. 99.
9. C. H. Townes and A. L. Schawlow, Microwave Spectroscopy, McGraw-Hill, New York (1955).
10. A. Ben-Reuven, Impact Broadening of Microwave Spectra, Phys. Rev. 145, 7 (1966); and Phys. Rev. Letters 14, 349 (1965).
11. B. Bleaney and J. H. N. Loubser, The Inversion Spectra of NH_3, CH_3Cl, and CH_3Br at High Pressures, Proc. Phys. Soc. 63A, 483 (1950).
12. A. A. Maryott (private communication).

13. G. T. Wrixon, Micorwave Absorption in the Jovian Atmosphere, Univ. of Calif. Lab. Rep., Ser. 10, issue 26 (1969).

14. B. A. Sodek Jr., J. Spacecraft and Rockets 5, 461 (1968).

15. Handbook of Chemistry and Physics, Chemical Rubber Co., Cleveland (1961).

16. D. E. Kerr ed., Propagation of Short Radio Waves, McGraw-Hill, New York (1951).

17. A. Kliore, et. al., Science 158, 1683 (1967).

18. G. Birnbaum, S. J. Kryder, and H. Lyons, J. Appl. Phys. 22, 95 (1951).

19. J. D. Jackson, Classical Electrodynamics, Wiley, New York (1962), p. 256.

20. G. Birnbaum and A. A. Maryott, Phys. Rev. 92, 270 (1953).

21. G. Birnbaum and A. A. Maryott, Jour. Chem. Phys. 21, 1774 (1953).

22. E. C. Morris and R. W. Parsons, Aust. Jour. Phys. 23, 335 (1970).

23. J. S. Lewis, Icarus 10, 365 (1969); Icarus 10, 393 (1969).

24. W. Ho, I. A. Kaufman, and P. Thaddeus, Jour. Geophys. Res. 71, 5091 (1966).

References 25 through 38 of RCA's Phase II report do not apply to this report and are, therefore, omitted. The numbering system of RCA's Phase II report (References 1 through 24, above) is kept intact. Additional references for this discussion begin with number 39.

39. C. G. Montgomery, Techniques of Microwave Measurements, vol. II of Rad. Lab. Series, McGraw-Hill, 1947.

40. W. Gordy, Rev. Modern Phys. 20, 668 (1948).

41. R. L. Cramer, Ames Research Center (NASA), Moffett Field, California (private communication).

42. W. Gordy, W. Smith, and R. Trambarulo, Microwave Spectroscopy, Wiley (1953).

43. W. H. Allen ed., Dictionary of Technical Terms for Aerospace Use, first edition, NASA SP-7 (1965).

44. R. P. Feynman, R. B. Leighton, and M. Sands, The Feynman Lectures on Physics, Volume I, Addison-Wesley, (1964).